



Motility and swimming: universal description and generic trajectories

Alexander Farutin^{1,a}, Suhail M. Rizvi^{1,2,b}, Wei-Fan Hu^{3,c}, Te-Sheng Lin^{4,d}, Salima Rafai^{1,e}, and Chaouqi Misbah^{1,f} 

¹ Univ. Grenoble Alpes, CNRS, LIPhy, F-38000 Grenoble, France

² Department of Biomedical Engineering, Indian Institute of Technology Hyderabad, Sangareddy, Telangana 502285, India

³ Department of Mathematics, National Central University, 300 Zhongda Road, Taoyuan 320, Taiwan

⁴ Department of Applied Mathematics, National Yang Ming Chiao Tung University, 1001 Ta Hsueh Road, Hsinchu 300, Taiwan

Received 25 September 2023 / Accepted 11 December 2023

© The Author(s), under exclusive licence to EDP Sciences, SIF and Springer-Verlag GmbH Germany, part of Springer Nature 2023

Abstract Autonomous locomotion is a ubiquitous phenomenon in biology and in physics of active systems at microscopic scale. This includes prokaryotic, eukaryotic cells (crawling and swimming) and artificial swimmers. An outstanding feature is the ability of these entities to follow complex trajectories, ranging from straight, curved (circular, helical...), to random-like ones. The non-straight nature of these trajectories is often explained as a consequence of the asymmetry of the particle or the medium in which it moves, or due to the presence of bounding walls, etc... Here, we show that for a particle driven by a concentration field of an active species, straight, circular and helical trajectories emerge naturally in the absence of asymmetry of the particle or that of suspending medium. Our proof is based on general considerations, without referring to an explicit form of a model. We show that these three trajectories correspond to self-congruent solutions. Self-congruency means that the states of the system at different moments of time can be made identical by an appropriate combination of rotation and translation of the coordinate space. We show that these solutions are exhibited by spherically symmetric particles as a result of a series of pitchfork bifurcations, leading to spontaneous symmetry breaking in the concentration field driving the particle motility. Self-congruent dynamics in one and two dimensions are analyzed as well. Finally, we present a simple explicit nonlinear exactly solvable model of fully isotropic phoretic particle that shows the transitions from a non-motile state to straight motion to circular motion to helical motion as a series of spontaneous symmetry-breaking bifurcations. Whether a system exhibits or not a given trajectory only depends on the numerical values of parameters entering the model, while asymmetry of swimmer shape, or anisotropy of the suspending medium, or influence of bounding walls are not necessary.

1 Introduction

Motility of microorganisms, such as eukaryotic and prokaryotic cells, as well as of their biomimetic counterparts, such as active particles and drops, constitutes today a fertile interdisciplinary topic. Consumption of energy and production of entropy enabling the motility make the traditional concepts of equilibrium statistical mechanics difficult to apply. These systems show a wide range of unexpected behaviors regarding both

their individual and collective dynamics, such as complex trajectories, non trivial patterns, and so on.

Living cells can swim in a fluid, crawl on a substratum or move in a complex environment (extracellular matrix, complex fluid, random media...) by using several strategies, such as shape changes (amoeboid motion), beating of cilia and flagellae, and so on [1–6]. It is recognized since more than a century that they (flagellate, spores, infusoria, and so on) have the ability to follow complex trajectories, such as spiral ones [7]. Other trajectories, like circular, helical, and even chaotic have been later identified for living cells and artificial particles [8–16]. These systems may combine intricate biochemical regulations, chemical and mechanical interactions, and nonlinear effects making their explicit elucidation quite challenging.

For many types of active particles, their shape and internal organization is what dictates the trajectory.

^a e-mail: alexander.farutin@univ-grenoble-alpes.fr

^b e-mail: suhair@bme.iith.ac.in

^c e-mail: wfhu@math.ncu.edu.tw

^d e-mail: teshenglin@nycu.edu.tw

^e e-mail: salima.rafai@univ-grenoble-alpes.fr

^f e-mail: chaouqi.misbah@univ-grenoble-alpes.fr
(corresponding author)

For example, a micro-alga *chlamydomonas reinhardtii* has an intrinsic asymmetry in its structure due to a pair of forward-facing flagella on its body. This asymmetry predetermines the swimming direction. Further asymmetry is added by the non-identical beating patterns of the two flagella, which results in a helix-like swimming trajectory. There are, however, active systems for which the motion direction is not predetermined by their structure. A prototypical example of such a system is given by Marangoni droplets, the motion of which is driven by surface gradients of a concentration field that they emit [15–24, 24–26]. At low enough emission rates, such droplets remain stationary and completely isotropic: they have a spherical shape, while the concentration field depends only on the distance from the particle. This state, however, can become unstable in favor of a motile solution, characterized by a steady motion of the droplet driven by an inhomogeneity of the concentration field along the droplet surface. This inhomogeneity is, in turn, sustained by the advection of the chemicals by the fluid flowing relative to the droplet. The transition to swimming occurs for such particles as a spontaneous symmetry breaking because the swimming direction can not be related to any feature of the stationary solution. Marangoni droplets belong to a more general class of autophoretic particles, which swim due to phoretic effects in solutes they emit. Another example of such particles is given by colloidal spheres that swim by catalyzing chemical reactions in the surrounding fluid.

The original theoretical works [17, 27, 28] assumed that autophoretic particles swim along a straight line with constant velocity. The experiments, however, have shown a variety of possible trajectories, such as circles, spirals, or even chaotically irregular trajectories. The occurrence of complex curved trajectories has been linked to the geometry of the particle (such as its chirality) [12], or to the nature of the suspending medium (complex fluid) [14], or to noise [29], or to the presence of bounding walls [3]. This has led to interesting descriptions of their motion. Surprisingly, complex motions have also been reported for isotropic particles (circular, spherical), where circular, meandering and chaotic motions are revealed in the absence of noise and bounding walls [16], pointing to their genericity.

Besides spherical autophoretic particles, other systems transition from stationary to motile states via spontaneous symmetry breaking. A notable example is given by amoeboid cells, which are round (circular on a 2D substrate, or spherical in a 3D medium) at rest but are polarized when they move [30–34]. The polarization is manifested as cell deformation from a spherical shape and the inhomogeneity of protein distributions along the cell surface. Cell motility can be directed by an external stimulus, such as a chemoattractant, or it can occur spontaneously, in which case the migration does not have a predetermined direction. The interplay between various ingredients involved in cell motility and swimming poses often a formidable challenge in terms of effective basic description and classification of their dynamics. At the same time it is expected that these

systems should obey some basic rules when formulated in a general framework based on symmetries and non equilibrium constraints (such as the lack of a variational formulation), regardless of the specific nature of the motile system under consideration.

Another related phenomenon is the formation and motion of concentration peaks in bulk active medium [35], which was also observed in epithelial tissue during embryo growth [36]. Similar dynamics arises in the study of active phase field crystals [37–39], where the patterns of the phase field can be used to model swarms of active particles.

Our focus here is the understanding of the emergence of generic curved trajectories for an initially isotropic, stationary active system. The present study focuses on the description of generic motions of a single entity driven by a chemical field (extensions to several fields will appear straightforward), be it crawling on a substrate, or moving in a fluid, without a specific reference to a system or to the environment in which it moves. By introducing a simple but a general framework where a particle is driven by a concentration field we will be able to state the general conditions under which a particle can transition from a non-motile to a motile state, and will identify the nature of the resulting bifurcation. We will identify the existence of generic types of motion that we will refer to as *self-congruent solutions*. These are solutions that keep the concentration field moving and rotating in a shape-preserving manner in the course of time. They correspond to three types of solutions: (i) straight trajectory, (ii) circular one, and (iii) helical ones. These solutions are identified on the basis of general symmetry properties.

The next step consists in writing explicitly, again based on symmetry, the evolution equations of the concentration fields components. It will appear that self-congruent solutions emerge naturally from explicit solutions of nonlinear equations. We will keep the equations simple enough, and we will show that retaining only two components (first two spherical harmonics) is sufficient to yield a complex picture. It turns out that these equations, though nonlinear, yield an exact solution describing the above three trajectory types. We will discuss here three motile systems, namely a segment in 1D, a circular particle in 2D and a spherical particle in 3D. This study highlights the potential of this framework which captures the main three essential motions in a unified way.

2 Problem formulation

The purpose of this work is to analyze the trajectories of self-propelling particles and the bifurcations which lead to transition from one trajectory type to another. We aim to consider this problem as generally as possible making little assumptions about the nature of the particle or the properties of the medium in which it moves. A typical example is a fluid described by the Stokes equations, as is often used for phoretic parti-

cles [16,17,19,21]. For this purpose, we assume that the motility of the particle is related to a concentration field $c(\mathbf{r}, t)$, which is a function of position \mathbf{r} and time t .

We consider two possibilities:

1. The particle is a material entity and the concentration field $c(\mathbf{r}, t)$ is distributed on the particle surface and, possibly, in the bulk media inside or outside the particle. Typical examples include Marangoni-driven particles [17, 19, 21], and acto-myosin assisted cell motility [32–34].
2. The particle is fictitious and refers to a feature of the concentration field $c(\mathbf{r}, t)$, such as a local maximum in \mathbf{r} for given t . For example, motion of peaks of myosin concentration in a tissue or phase field crystals belong to this case.

2.1 Material autophoretic particles

In the first case, we consider the dynamics of the active concentration field $c(\mathbf{r}, t)$ and of a set of additional scalar fields that are necessary to fully describe the state of the system. Taking a Marangoni droplet as an example, the shape and position of the particle can be represented by a phase-field ρ , which is equal to -1 outside the particle, 1 inside, and 0 on the boundary. We thus get a set of two scalar fields, the concentration and the phase field, which fully describe the state of the particle in an infinite fluid. Setting the particle shape and position along with the distribution of solute concentration in the fluid at some moment of time allows one to compute the state of the system at any following moment (as shown in “Appendix A” and in [16]).

Under this assumption, the time-dynamics of $\rho(\mathbf{r}, t)$ and $c(\mathbf{r}, t)$ is described by the following equations

$$\begin{aligned} \dot{\rho}(\mathbf{r}, t) &= \mathcal{F}\{\mathcal{T}_t\{\rho\}, \mathcal{T}_t\{c\}\}(\mathbf{r}) \equiv \mathcal{F}\{\rho(\mathbf{r}', t), c(\mathbf{r}', t)\}(\mathbf{r}), \\ \dot{c}(\mathbf{r}, t) &= \mathcal{G}\{\mathcal{T}_t\{\rho\}, \mathcal{T}_t\{c\}\}(\mathbf{r}) \equiv \mathcal{G}\{\rho(\mathbf{r}', t), c(\mathbf{r}', t)\}(\mathbf{r}), \end{aligned} \tag{1}$$

where \mathcal{F} and \mathcal{G} are non-linear operators and the dot refers to partial derivative with respect to time. The time substitution operator \mathcal{T}_t takes a time-dependent field and returns a function of the space coordinate alone by evaluating the field at time equal to t :

$$\mathcal{T}_t\{\rho\}(\mathbf{r}) = \rho(\mathbf{r}, t), \quad \mathcal{T}_t\{c\}(\mathbf{r}) = c(\mathbf{r}, t). \tag{2}$$

The operator \mathcal{G} takes two functions of coordinate \mathbf{r}' and returns a third function of \mathbf{r}' . The expression $\mathcal{G}\{\mathcal{T}_t\{\rho\}, \mathcal{T}_t\{c\}\} \equiv \mathcal{G}\{\rho(\mathbf{r}', t), c(\mathbf{r}', t)\}$ in (1) is used to denote the function returned by the operator \mathcal{G} applied to the functions $\mathcal{T}_t\{\rho\}$ and $\mathcal{T}_t\{c\}$ defined by (2). Sampling the function $\mathcal{G}\{\rho', c'\}$ at a given point \mathbf{r} is denoted as $\mathcal{G}\{\rho', c'\}(\mathbf{r})$ for arbitrary functions ρ' and c' of the space coordinate. The value of \dot{c} at some point \mathbf{r} and time t is thus a non-linear function of the values of $c(\mathbf{r}', t)$ and $\rho(\mathbf{r}', t)$ at all possible points \mathbf{r}' but the same time t . In other words, the evolution equations

(1) are nonlocal in space but local in time. Similarly, the operator \mathcal{F} represents the evolution of the phase field, which encodes the deformation and translation of the particle. The notation (1) thus codifies that the evolutions of concentration and particle shape and position can be unambiguously reconstructed from the instantaneous concentration and phase fields. Since the problem we consider here is local in time, the dependence on t is implied below, whenever such simplification of notations does not lead to confusion.

The following analysis does not depend on the explicit expressions of the operators \mathcal{F} and \mathcal{G} , relying only on their symmetry properties. This symmetry reflects the invariance of the problem under rotations and translations of the underlying space. That is, if we define an isometry operator Γ such that for any field $c'(\mathbf{r})$

$$\Gamma\{c'\}(r) = c'(R \cdot \mathbf{r} + \mathbf{r}_0) \tag{3}$$

for an arbitrary orthogonal matrix R and translation vector \mathbf{r}_0 , we can write

$$\begin{aligned} \mathcal{G}\{\Gamma\{\rho'\}, \Gamma\{c'\}\} &= \Gamma\{\mathcal{G}\{\rho', c'\}\}, \\ \mathcal{F}\{\Gamma\{\rho'\}, \Gamma\{c'\}\} &= \Gamma\{\mathcal{F}\{\rho', c'\}\}. \end{aligned} \tag{4}$$

Here the fields ρ' and c' can be arbitrary functions of the space coordinate.

The non-motile state of autophoretic particles is characterized by rotational symmetry about the particle center: Marangoni droplets are spherical at rest, and the concentration field emitted by a stationary particle depends only on the distance from the particle center. Similarly, non-motile cells have a round shape with proteins responsible for their motility distributed homogeneously along the cell surface. It turns out that the existence of these symmetric stationary solutions is a generic consequence of the symmetry (4): Namely, if the functions $c(\mathbf{r}, t)$ and $\rho(\mathbf{r}, t)$ depend only on the distance from the particle center for $t = 0$, Eqs. (4) guarantee that this rotational symmetry is preserved for every $t > 0$. The non-motile states are prevalent in the limit of low system activity because the dissipative effects tend to homogenize the concentration field c as much as the presence of the particle allows this. At higher activity, however, the rotational symmetry can be spontaneously broken, which can lead to particle motility.

2.2 Fictitious particle

In the case of material autophoretic particles, the presence of the particle introduces an inherent inhomogeneity in the concentration field. Another possibility for an inhomogeneity of c to appear is via spontaneous symmetry breaking of a homogeneous solution. If this leads to an emergence of an isolated spot of increased or reduced concentration, this spot can be viewed as a fictitious particle. As in the case of material particles, an initially rotationally symmetric spot remains rotationally symmetric at any time and does not move. This

corresponds to a stationary solution for autophoretic particles. However, other solutions can exist, in which the concentration spot is changing its position and, possibly, orientation over time. If such a solution preserves the shape of the spot, the spot will be seen in this study as a moving fictitious particle.

2.3 Model

In the following, we focus on the dynamics of the concentration field $c(\mathbf{r}, t)$, assuming that the dynamics of all other scalar fields describing the particle can be reconstructed from the concentration field dynamics. The following analysis can also be repeated for a system described by several scalar fields, at a price of more cumbersome notation. As is shown below, the one-field model is sufficient to describe the emergence of straight, circular and helical trajectories. Obviously, the same mechanism can lead to emergence of non-straight trajectories for active particles described by more than one scalar field (like concentration c and phase field ρ for autophoretic droplets).

Since this work considers spontaneous symmetry breaking of the concentration field, the shape of the particle is taken to be invariant under rotations. Namely, we consider the following 3 cases:

- 1D case: a segment particle on a line
- 2D case: a circular particle in a plane
- 3D case: a spherical particle in a space

For the concentration field c , this corresponds to a spot of concentration excitation having the same symmetry as the particle for low enough activity. This spot of concentration can appear due to the presence of a material active particle or spontaneously, as described above.

Equations (1) are simplified to

$$\dot{c}(\mathbf{r}, t) = \mathcal{G}\{\mathcal{I}_t\{c\}\}(\mathbf{r}) \quad (5)$$

by eliminating the secondary scalar fields. The symmetry relation is simplified to

$$\mathcal{G}\{\Gamma\{c\}\} = \Gamma\{\mathcal{G}\{c\}\}. \quad (6)$$

For material particles, the velocity $\mathbf{v}(t)$ is a well-defined quantity and can be calculated as a function of the particle position and the concentration field [16, 17, 19, 21]. This is not the case, in general, for fictitious particles, which do not have a well-defined position. Here we consider only the case when the shape of the concentration spot defining the fictitious particle is preserved in time. In this case, the particle velocity $\mathbf{v}(t)$ can be reconstructed from the time-evolution of the concentration field c , as explained below.

Since we do not define explicitly the motility mechanism in our model, we use a generic Péclet number Pe as a measure of the activity of the system. This number relates the active power injected into the system to

the passive dissipation. Depending on the problem, the dissipative effects relate to the diffusion of the active species, which tends to even out the concentration field c , the viscosity of the medium outside the particle, and so on. The particle activity is driven by Marangoni stresses for autophoretic droplets or contractility of the myosin molecular motors for cells. The changes of Pe affect the system dynamics, expressed by Eq. (5). This implies that the operator \mathcal{G} in (5) is a function of Pe .

The goal of this work is to analyze which particle trajectories can appear in the proposed model. We consider the symmetry breaking bifurcations which separate different motile states from each other and from the static case.

3 Self-congruent solutions

Self-similar solutions play an important role in many physical problems. Along this line, we analyze a related class of solutions, which we call self-congruent solutions below. We call a solution self-congruent if the concentration fields at different moments of time can be made identical by an appropriate composition of rotation and translation of the space (congruence transformation). In other words, concentration dynamics is self-congruent if there exists an appropriately moving and rotating reference frame in which the concentration field is independent of time. We choose the name by analogy with a widely used term of self-similar solution, for which the states at different moments of time can be made identical by a scaling transformation of the space. We present in this Section the possible types of self-congruent solutions and analyze the resulting trajectories of the particle. The next Section is dedicated to the discussion of how self-congruent solutions emerge from the non-motile state through a series of pitchfork bifurcations as the activity is increased.

The formal expression of self-congruency reads

$$c(\mathbf{r}, t) = \Gamma_t\{C\}(\mathbf{r}), \quad (7)$$

where $C(\mathbf{r}')$ is a time-independent reference concentration field and Γ_t is a time-dependent isometry operator, defined by a time-dependent rotation matrix $R(t)$ and a time-dependent offset vector $\mathbf{r}_c(t)$:

$$\Gamma_t\{c'\}(r) = c'[R(t) \cdot (\mathbf{r} - \mathbf{r}_c(t))] \quad (8)$$

for any field c' . This means that the concentration field moves in a shape-preserving manner, very much like the usual travelling-wave solution equation. This also means that two concentration fields at two different times can be made identical to each other via an appropriate translation and rotation. The reference concentration field C in (7) does not depend on time. Time only enters the right hand side of Eq. (7) through $R(t)$ and $\mathbf{r}_c(t)$.

According to (7) the trajectory of the particle is fully determined by the time dependence of $R(t)$ and $\mathbf{r}_c(t)$ for

self-congruent solutions. The symmetry (6) prescribes the possible behaviors of $R(t)$ and $\mathbf{r}_c(t)$: Measuring $\dot{R}(t)$ and $\dot{\mathbf{r}}_c(t)$ as a function of $R(t)$ for some moment of time t , allows us to reconstruct $\dot{R}(t')$ and $\dot{\mathbf{r}}_c(t')$ as a function of $R(t')$ for an arbitrary time t' by performing an appropriate rotation. This effectively defines the time-evolution of a self-congruent solution by a combination of an angular velocity measuring the rotation of the co-rotating frame and a translational velocity, as proven below. A straightforward calculation, also given below, shows that this limits the possible trajectories in self-congruent solutions to fixed point, straight line, circle, and helix.

We start the proof by substituting the ansatz (7) into the dynamics equation (5):

$$[\dot{R}(t) \cdot (\mathbf{r} - \mathbf{r}_c(t)) - R(t) \cdot \dot{\mathbf{r}}_c(t)] \cdot \Gamma_t\{\nabla C\} = \mathcal{G}\{\Gamma_t\{C\}\} = \Gamma_t\{\mathcal{G}\{C\}\}, \tag{9}$$

where ∇C is the gradient of $C(\mathbf{r})$. The last equality in (9) is obtained by using the commutativity of the non-linear operator \mathcal{G} with rotations and translations of the space (6). We now define a matrix $\Omega(t)$, which is nothing but the angular velocity matrix of the corotating frame, expressed in the corotating frame, such that

$$\dot{R}(t) = \Omega(t) \cdot R(t). \tag{10}$$

It follows from taking the time derivative of the orthogonality condition $R(t) \cdot R(t)^T = I$, where I is the identity matrix that $\Omega(t)^T = -\Omega(t)$, whence we write

$$\Omega_{ij}(t) = \epsilon_{ijk}\omega_k(t), \tag{11}$$

where ϵ is the Levi-Civita symbol and $\boldsymbol{\omega}(t)$ is the angular velocity of the co-rotating frame.

We further define a vector $\mathbf{v}(t)$ (which is the velocity of the particle in the co-rotating frame) such that

$$R(t) \cdot \dot{\mathbf{r}}_c(t) = \mathbf{v}(t). \tag{12}$$

Substituting the definitions (10) and (12) into the left hand side of (9) yields

$$[\Omega(t) \cdot R(t) \cdot (\mathbf{r} - \mathbf{r}_c(t)) - \mathbf{v}(t)] \cdot \Gamma_t\{\nabla C\} \equiv \Gamma_t\{\boldsymbol{\omega}(t) \times \mathbf{r} - \mathbf{v}(t)\} \cdot \Gamma_t\{\nabla C\} = \Gamma_t\{[\boldsymbol{\omega}(t) \times \mathbf{r} - \mathbf{v}(t)] \cdot \nabla C\}, \tag{13}$$

where the last equality is valid because of the commutativity of the algebraic operations on fields with the isometry operator Γ_t . Substituting (13) into Eq. (9), and removing Γ_t (by applying the inverse coordinate transform) from both sides, we obtain

$$[\boldsymbol{\omega}(t) \times \mathbf{r} - \mathbf{v}(t)] \cdot \nabla C = \mathcal{G}\{C\}. \tag{14}$$

Note that the right hand side of (14) is independent of t . This implies that the expression $[\boldsymbol{\omega}(t) \times \mathbf{r} - \mathbf{v}(t)] \cdot$

$\nabla C(\mathbf{r})$ in (9) is also independent of t . Taking the difference of this expression at two moments, t_1 and t_2 , we get

$$0 = [\boldsymbol{\omega}(t_1) \times \mathbf{r} - \mathbf{v}(t_1)] \cdot \nabla C(\mathbf{r}) - [\boldsymbol{\omega}(t_2) \times \mathbf{r} - \mathbf{v}(t_2)] \cdot \nabla C(\mathbf{r}) = [\Delta\boldsymbol{\omega} \times \mathbf{r} - \Delta\mathbf{v}] \cdot \nabla C(\mathbf{r}) = \Delta\boldsymbol{\omega} \cdot [\mathbf{r} \times \nabla C(\mathbf{r})] - \Delta\mathbf{v} \cdot \nabla C(\mathbf{r}), \tag{15}$$

where $\Delta\boldsymbol{\omega} = \boldsymbol{\omega}(t_1) - \boldsymbol{\omega}(t_2)$ and $\Delta\mathbf{v} = \mathbf{v}(t_1) - \mathbf{v}(t_2)$. Because Eq. (15) is valid for all \mathbf{r} , either $\Delta\boldsymbol{\omega} = 0$ and $\Delta\mathbf{v} = 0$ or there is a linear relation between the components of two vector fields $\nabla C(\mathbf{r})$ and $\mathbf{r} \times \nabla C(\mathbf{r})$. The latter option is only possible for particular symmetries of the concentration field C : For example, if C is a rotationally invariant field that depends only on the distance from the origin, $\nabla C(\mathbf{r}) \propto \mathbf{r}$ for all \mathbf{r} . In this case, $\mathbf{r} \times \nabla C(\mathbf{r}) = 0$ and (15) is thus satisfied for any $\Delta\boldsymbol{\omega}$. Since the particle is stationary for a rotationally invariant concentration field, this ambiguity of the angular velocity of the co-rotating reference frame is expected. Similarly, if the concentration field is invariant with respect to rotations about z axis, $\Delta\omega_z$ is undefined. Finally, if the concentration field is invariant with respect to translations along z axis, Δv_z is undefined and neither $\Delta\boldsymbol{\omega}$ nor $\Delta\mathbf{v}$ can be defined for a position-independent concentration field.

Excluding the special cases discussed above, we obtain that $\Delta\boldsymbol{\omega} = 0$ and $\Delta\mathbf{v} = 0$, which means that $\boldsymbol{\omega}(t)$ and $\mathbf{v}(t)$ are actually constant in time. From this observation we write $\boldsymbol{\omega}(t) = \boldsymbol{\omega}^0$, $\mathbf{v}(t) = \mathbf{v}^0$. Note that the angular velocity $\boldsymbol{\omega}$ defined here refers to the dynamics of the concentration field c and, in general, does not correspond to an actual rotation of the material particle. For example, it is known [16] that Marangoni flows do not contribute to rotation for spherical or circular droplets but rotating self-congruent solutions appear for them nevertheless.

An intuitive explanation of the above derivation can be given as follows: C corresponds to the concentration field in the frame of reference comoving and corotating with the concentration field. Since this field is time-constant, all functions associated with it should also be constant in the comoving and corotating frame. In particular, the velocity and the angular velocity of the fixed laboratory frame should also be constant when measured and expressed in the comoving and corotating frame. The vectors $-\mathbf{v}^0$ and $-\boldsymbol{\omega}^0$ represent these constants.

Integrating (10) yields

$$R(t) = \exp(\Omega^0 t) \cdot R(0). \tag{16}$$

For simplicity, we choose the axes in the corotational frame to coincide with the axes of the laboratory frame at $t = 0$. The matrix $R(0)$ is the identity matrix in this case. We choose the z axis as the direction of $\boldsymbol{\omega}$ at $t = 0$. The matrix Ω then has only two non-zero components for this choice of axes: $\Omega_{xy} = -\Omega_{yx} = \omega^0$. Its exponent

then reads

$$\exp(\Omega^0 t) = \begin{pmatrix} \cos \omega^0 t & \sin \omega^0 t & 0 \\ -\sin \omega^0 t & \cos \omega^0 t & 0 \\ 0 & 0 & 1 \end{pmatrix}, \quad (17)$$

which corresponds to a usual rotation matrix. We can now solve for the propulsion velocity

$$\dot{\mathbf{r}}_c(t) = \mathbf{R}(t)^{-1} \cdot \mathbf{v}^0 = v_x^0 (\mathbf{e}^x \cos \omega^0 t + \mathbf{e}^y \sin \omega^0 t) + v_z^0 \mathbf{e}^z, \quad (18)$$

where we have chosen the y axis at $t = 0$ in such a way that $v_y^0 = 0$. $\mathbf{e}^x, \mathbf{e}^y, \mathbf{e}^z$ are unit vectors along the corresponding directions.

Let us now analyze the possible dynamics defined by Eq. (18) and the resulting trajectories. The simplest case corresponds to $v_x^0 = v_z^0 = 0$, whence $\dot{\mathbf{r}}_c = 0$. The particle is stationary in this case. The next possibility is $v^0 \neq 0$ and $\omega^0 = 0$. The velocity (18) is constant in time in this case. The trajectory of the particle is a straight line. Next, we consider the case $v_x^0 \neq 0, \omega^0 \neq 0$ and $v_z^0 = 0$. The velocity is time-dependent in this case. It always lies in the (x, y) plane and rotates about the z axis with a constant angular velocity ω^0 . The corresponding trajectory is a circle in the (x, y) plane. The particle traces a full circle in time $2\pi/\omega^0$, during which time it travels a distance of $2\pi v_x^0/\omega^0$. This corresponds to a circle of radius v_x^0/ω^0 . Finally, if $v_x^0 \neq 0, \omega^0 \neq 0$, and $v_z^0 \neq 0$, then the velocity in the laboratory frame has a rotating component in the (x, y) plane and a constant component along the z axis. Integrating the velocity in time shows that the trajectory corresponds to a helix, whose axis is parallel to z axis. The period of the rotating component is $2\pi/\omega^0$, during which time the particle projection on the (x, y) plane travels a distance of $2\pi v_x^0/\omega^0$. This implies that the radius of the helix is v_x^0/ω^0 . The distance traveled along the z axis during one period is $2\pi v_z^0/\omega^0$, which sets the pitch of the helix. The following expressions of the helix radius a and the pitch $2\pi b$ can be used for an arbitrary choice of the coordinates:

$$a = \frac{|\mathbf{v}^0 \times \boldsymbol{\omega}^0|}{(\omega^0)^2}, \quad 2\pi b = 2\pi \frac{\mathbf{v}^0 \cdot \boldsymbol{\omega}^0}{(\omega^0)^2}. \quad (19)$$

The trajectory type is related to the symmetry of the reference concentration field $C(\tilde{\mathbf{r}})$. Namely, if any transformation of the space keeps C invariant, the vectors \mathbf{v}^0 and $\boldsymbol{\omega}^0$ should also be unchanged by this transformation. It is important to note that vector \mathbf{v}^0 is polar, while the vector $\boldsymbol{\omega}^0$ is axial, that is the former changes sign on inversion of the space and the latter is unaffected by it. Consider now the 4 trajectory types: In non-motile state both vectors are zero, so the symmetry of the $(\mathbf{v}^0, \boldsymbol{\omega}^0)$ tuple is the full $O(3)$ group. Straight trajectory corresponds to $\omega^0 = 0$, so the symmetry group is $C_{\infty v}$, which corresponds to arbitrary rotations about the \mathbf{v}^0 direction and also reflection with respect to any plane containing \mathbf{v}^0 . The circular trajectory corresponds to a single mirror symmetry (group C_s) with

respect to the plane containing \mathbf{v}^0 and orthogonal to $\boldsymbol{\omega}^0$ (as it is an axial vector). This mirror plane defines the plane in which the circle is drawn. Finally, the vectors \mathbf{v}^0 and $\boldsymbol{\omega}^0$ are not orthogonal for helical trajectories, which leaves the symmetry group of the system trivial.

Phoretic particles in lower dimensions can exhibit a subset of the 4 trajectory types described above: Stationary particle, straight and circular motions in 2D, or stationary particle and straight motion in 1D.

4 Emergence of self-congruent solutions

The question arises of whether self-congruent solutions are just a mathematical curiosity, or whether they emerge naturally in a given motility model. It will appear here and in subsequent sections that self-congruent solutions are the rule. In this Section we analyze the emergence of motile self-congruent solutions from a stationary state and the bifurcations which mark the transitions from one trajectory type to another. Our starting point is the evolution equation (5). We first consider the simplest case of 1D phoretic system and then show how the dynamics in two or more dimensions can be reduced to the 1D case.

4.1 1D case: segment particle on a line

4.1.1 Stationary solution

The 1D case corresponds to a distribution of concentration $c(x, t)$ along the line $x \in (-\infty, \infty)$. A related discussion can be found in [39] in application to a particular equation governing a phase field crystal in 1D. We take the particle as a segment which runs from $x = x_c - 1$ to $x = x_c + 1$, where x_c is the position of the particle. We place initially the particle in the origin, such that $x_c = 0$ at $t = 0$. The functional dependence of the time evolution of the concentration field for its given distribution is given by Eq. (5), where $c(\mathbf{r}, t)$ reduces to $c(x, t)$. There are two symmetries that the dependence (5) must satisfy in 1D: the translational invariance

$$\mathcal{G}\{c(x' + x_0)\}(x) = \mathcal{G}\{c(x')\}(x + x_0) \quad (20)$$

for arbitrary x_0 and the change of sign of x :

$$\mathcal{G}\{c(-x')\}(x) = \mathcal{G}\{c(x')\}(-x), \quad (21)$$

both for an arbitrary instantaneous concentration field $c(x)$.

We first take the limit of low activity Pe , which corresponds to a ground state $c_0(x)$ of the concentration distribution. It is natural to assume that this distribution is symmetric $c_0(-x) = c_0(x)$ about its center $x_c = 0$ and thus by symmetry the particle is not motile. By definition (stationary solution), $\mathcal{G}\{c_0(x')\} = 0$. The next step is to analyze the linear stability of this solution. We introduce a small instantaneous perturbation

of the concentration field $\varepsilon\delta c(x)$, where ε is an arbitrary small number, used here to highlight the smallness order of different terms. The function $\delta c(x)$ is considered to be of order of 1. Note that $\delta c(x)$ is a function of x alone. No time dependence is implied here because this function is used to analyze the properties of the operator \mathcal{G} , which is local in time.

Taking $c(x) = c_0(x) + \varepsilon\delta c(x)$, we can write

$$\mathcal{G}\{c_0(x') + \varepsilon\delta c(x')\}(x) = \varepsilon\mathcal{G}_1\{\delta c(x')\}(x) + O(\varepsilon^2), \tag{22}$$

where \mathcal{G}_1 is a linear operator. The linear stability of the solution $c_0(x)$ is thus related to the eigenvalues of the linear operator \mathcal{G}_1 . Further below, we use λ_i and $f_i(x)$ to denote the eigenvalues and the corresponding eigenfunctions of the linear operator \mathcal{G}_1 . Here the index i is supposed to run from 0 to ∞ . Note that functions $f_i(x)$ are defined on the x space and thus have no time variable because the operator \mathcal{G}_1 is local in time. It is important for our analysis that the set of eigenvalues be discrete, at least for eigenvalues close to zero. This is usually the case for systems of finite size, as happens for autophoretic particles in a finite fluid domain or for myosin-induced motility in which the myosin is localized within the cell cortex. Most importantly, the eigenvalue spectrum is discrete for problems defined on a circle or on a sphere. The eigenfunctions are given by Fourier harmonics or spherical harmonics, respectively, in these two cases, with eigenvalues following a more or less regular function of the harmonic order. These two cases of finite domain will be used in our analysis of the possible trajectories in 2D and in 3D.

An important property of the eigenfunctions $f_i(x)$ is that they are either symmetric or antisymmetric with respect to the transformation $x \rightarrow -x$. This is a consequence of the symmetry of the operator \mathcal{G}_1 and the solution $c_0(x)$. Indeed if \mathcal{P} is the inversion operator (which commutes with \mathcal{G}_1 , and thus has common eigenmodes), it obeys $\mathcal{P}^2 = \mathcal{I}$ (where \mathcal{I} is the identity operator), meaning that its eigenvalues obey $\lambda^2 = 1$ ($\lambda = \pm 1$). Consequently, since by definition $\mathcal{P}f_i(x) = f_i(-x) = \lambda f_i(x)$, and because $\lambda = \pm 1$, we get for all eigenstates i either $f_i(-x) = f_i(x)$ or $f_i(-x) = -f_i(x)$.

One eigenvalue of \mathcal{G}_1 is special and is equal to zero for any Pe . This eigenvalue corresponds to the homogeneous translation of the concentration field. Indeed, substituting $c(x) = c_0(x + \varepsilon) = c_0(x) + \varepsilon\partial_x c_0(x) + O(\varepsilon^2)$ for an arbitrary small value ε (meaning $\delta c(x) = \partial_x c_0(x)$) in Eq. (22), and using $\mathcal{G}\{c_0(x + \varepsilon)\} = \mathcal{G}\{c_0(x)\} = 0$, we get

$$\mathcal{G}_1\{\partial_x c_0(x')\}(x) = 0. \tag{23}$$

That is, the eigenfunction $\partial_x c_0(x)$ corresponds to the eigenvalue 0. Further below, we use index 0 for this eigenvalue ($\lambda_0 = 0$, $f_0(x) = \partial_x c_0(x)$). Note that, in general, this property of $\partial_x c_0(x)$ is unique. Higher order terms in ε -expansion of $\mathcal{G}\{c_0(x' + \varepsilon)\} = 0$ yield additional identities but these identities are non-linear and

thus do not provide further insight into the eigenfunctions of \mathcal{G}_1 .

4.1.2 Critical activity and the importance of non self-adjoint operator \mathcal{G}_1

The solution $c_0(x)$ is linearly stable provided all eigenvalues other than 0 have negative real parts. We now analyze the change of the dynamics of the system as one of the eigenvalues goes from negative to positive while the real parts of all the other eigenvalues remain negative. Suppose we have an eigenvalue λ_1 and a critical activity Pe_1 such that $\lambda_1(Pe_1) = 0$. We also consider the case when the eigenfunction f_1 is antisymmetric, so that the symmetry of the system changes at $Pe = Pe_1$. The goal of the following discussion is to show that the dynamics of the particle undergoes a pitchfork bifurcation at $Pe = Pe_1$ and that if the bifurcation is supercritical the concentration field for $Pe > Pe_1$ corresponds to a self-congruent solution with translational velocity $v^0 \propto (Pe - Pe_1)^{1/2}$.

The operator \mathcal{G}_1 has two eigenvalues equal to 0 for $Pe = Pe_1$. Only if the operator \mathcal{G}_1 is self-adjoint, can it be fully diagonalized for $Pe = Pe_1$. This would be the case, for example, if the problem were variational (global thermodynamical equilibrium). In active systems the evolution equation (5) is non-variational and the linearized operator is generically not self-adjoint. This will have important consequences as seen below. Non self-adjoint operator \mathcal{G}_1 with a degenerate eigenvalue is called defective. It can not be fully diagonalized.

In the case of non self-adjoint operator, with a doubly degenerate eigenvalue ($\lambda = 0$), we use the Jordan normal form to analyze the linear dynamics of the system: Equation (23) remains valid for $Pe = Pe_1$ because it represents a symmetry of the problem. In the Jordan spirit, if $f_0(x)$ is an eigenfunction associated to a zero eigenvalue (and it is so as we have shown above), then another function $f_1(x)$ satisfies $\mathcal{G}_1\{f_1(x')\}(x) = f_0(x) \equiv \partial_x c_0(x)$ for $Pe = Pe_1$. The function $f_1(x)$ is called a generalized eigenfunction. Substituting $c(x, t) = c_0(x) + \varepsilon\delta c_1(t)f_1(x)$ in (22), where $\delta c_1(t)$ is the time-dependent amplitude of the perturbation, we get

$$\dot{c}(x, t) = \varepsilon\delta c_1(t)\partial_x c_0(x) + O(\varepsilon^2). \tag{24}$$

The form of Eq. (24) is that of an advection equation, the general solution of which does not depend on x and t separately, but on $x - v_0t$ (v_0 is a constant). To leading order the concentration field reads

$$c(x, t) = c_0(x - v_0t) + \varepsilon\delta c_1(t)f_1(x - v_0t) + O(\varepsilon^2). \tag{25}$$

The concentration evolution equation then reads

$$\begin{aligned} -v^0\partial_x c_0(x - v^0t) + \varepsilon\delta\dot{c}_1(t)f_1(x - v_0t) \\ = \varepsilon\delta c_1(t)\partial_x c_0(x - v^0t) + O(\varepsilon^2), \end{aligned} \tag{26}$$

whence, by separating the $f_0(x - v^0t)$ and $f_1(x - v^0t)$ components, $v^0 = -\varepsilon\delta c_1(t)$ and $\delta\dot{c}_1(t) = O(\varepsilon)$. This confirms that for $Pe = Pe_1$ the solution (25) is marginally stable and would move in the negative x direction with velocity $\varepsilon\delta c_1(t)$. Thus the first type of motile self-congruent solutions (motion at constant velocity) emerges here naturally. Note that if the linear operator were self-adjoint, then we would have $\mathcal{G}_1\{f_1(x')\} = 0$ at bifurcation point, and the right hand side of (26) would be zero, and so would be the swimming speed. Note also that if the nonlinear operator \mathcal{G} (Eq. (5) is a functional derivative of some functional (implying automatically that the linear operator is self-adjoint) then there is no swimming. A general proof is given in ‘‘Appendix B’’.

4.1.3 Above critical activity

The next step is to solve the problem for positive values of $Pe - Pe_1$ in order to find the steady-state value of $\delta c_1(t)$ as a function of Pe . The eigenvalues λ_0 and λ_1 of the operator \mathcal{G}_1 are distinct for $Pe \neq Pe_1$ and it can thus be fully diagonalized. However, the eigenvectors f_0 and f_1 are almost identical (up to a scale factor) as Pe tends to Pe_1 . A basis containing these vectors is therefore not particularly suitable for representing the solution close to the bifurcation point. Instead, we use the generalized eigenfunctions of the operator \mathcal{G}_1 evaluated at $Pe = Pe_1$ to parametrize the solution. These functions are thus independent of Pe , while the operator \mathcal{G}_1 undergoes a regular perturbation at the bifurcation point. This choice of the basis functions makes the calculations straightforward but the expressions remain quite involved. We therefore give here only the main idea of the derivation while the details are given in ‘‘Appendix C’’.

The concentration field is written as

$$c(x, t) = c_0(x - x_c(t)) + \varepsilon\delta c_1(t)f_1(x - x_c(t)) + \varepsilon^2 \sum_{i=2}^{\infty} \delta c_i(t)f_i(x - x_c(t)) \tag{27}$$

in the comoving frame. Here $x_c(t)$ sets the position of the particle. The expansion (27) represents the concentration field as a sum of the non-motile solution and a perturbation, which is expanded in the basis of the generalized eigenfunctions of the operator \mathcal{G}_1 . Note that the function $f_0(x)$ is missing from the expansion (27). Its role is taken by the variable position $x_c(t)$. This allows us to convert the evolution of the continuous concentration field into a discrete system of ordinary differential equations. Namely, $\mathcal{G}\{c(x, t)\}$ is expanded into the basis defined by the functions f_i , which gives the time derivatives of $x_0(t)$ and $\delta c_i(t)$. Next we derive a closed evolution equation for $\delta c_1(t)$. This can be done by so-called adiabatic elimination of the rapidly decaying modes in the concentration perturbation (see [40] for a practical example of this technique). Indeed, the phoretic system has two distinct time scales close to

the critical activity: One corresponds to the evolution of $\delta c_1(t)$, the growth rate of which is proportional to $Pe - Pe_1$ and thus can be arbitrary small close enough to the transition point. The other time scale is defined by the smallest of $|\lambda_i|$ for all $i > 1$, which sets the decay rate of the stable modes. The latter time scale remains finite at the transition point. The adiabatic elimination proceeds in the following way:

1. We fix a value of δc_1 .
2. We solve the time evolution equations for $\delta c_i(t)$ for $i > 1$ with this value of δc_1 .
3. We obtain the steady-state values to which $\delta c_i(t)$ relax after an initial transient.
4. We call these saturation values as $\delta c_i^0(\delta c_1)$ (for $i > 1$).
5. We substitute the values $\delta c_i^0(\delta c_1)$ in equations for $\delta\dot{c}_1(t)$ and $\dot{x}_c(t)$.

The above procedure converges to fixed values of $\delta c_i^0(\delta c_1)$ for sufficiently small ε and $Pe - Pe_1$ because all modes $f_i(x)$ for $i > 1$ are stable in a sufficiently narrow region around $Pe = Pe_1$. The values $\delta c_i^0(\delta c_1(t))$ agree with the actual solution $\delta c_i(t)$ to the leading order thanks to the separation of time scales. In particular, $\delta c_i^0(\delta c_1(t))$ is equal to $\delta c_i(t)$ exactly for steady-state solutions.

Once the adiabatic elimination is applied, the time evolution equation for $\delta c_1(t)$ can be expanded as:

$$\varepsilon\delta\dot{c}_1(t) = a_1\varepsilon\delta c_1(t) + a_3\varepsilon^3\delta c_1(t)^3 + O(\varepsilon^5). \tag{28}$$

The coefficients for even powers in expansion (28) vanish because the function $f_1(x)$ is odd, so that the concentration field must be invariant under transformation $(x, \varepsilon, t) \rightarrow (-x, -\varepsilon, t)$, which in the case of Eq. (28) reduces to $\varepsilon \rightarrow -\varepsilon$ invariance. The coefficient a_1 is proportional to $Pe - Pe_1$ close to the bifurcation point. If the coefficient a_3 is negative, Eq. (28) has two stable fixed points $\varepsilon\delta c_1^0 = \pm(-a_1/a_3)^{1/2} \propto (Pe - Pe_1)^{1/2}$. This defines a supercritical pitchfork bifurcation. Equation (26) remains valid to the leading order even for $Pe > Pe_1$, which implies $\dot{x}_c(t) = -\varepsilon\delta c_1(t) + o(\varepsilon)$. The presented analysis shows that the concentration evolution equation has a stable self-congruent solution of form (25) with velocity proportional to $(Pe - Pe_1)^{1/2}$. ‘‘Appendix C’’ provides an explicit calculation.

4.2 2D case: circular particle in a plane

A generic example of the bifurcation dynamics in a 2D autophoretic system is considered in [40]. Among the bifurcations presented in that work, two correspond to transitions to self-congruent dynamics: The first one marks transition from a stationary isotropic concentration field around the particle to a polarized concentration field and straight motion of the particle. The concentration field retains a mirror symmetry after this bifurcation. The second bifurcation marks transition from straight to circular trajectories. The concentration

field loses its mirror symmetry at this bifurcation. Here we show how these observations can be explained in the general framework of the self-congruent solutions.

4.2.1 Primary bifurcation

For the 2D case we consider a concentration field $c(x, y)$ defined on a plane. It is convenient to introduce a comoving polar coordinate system by associating the center of the particle with the origin. For low enough Pe , the concentration field is rotationally symmetric and thus is a function of distance from the center r , $c_0(x, y) = c_0(r)$. This corresponds to the non-motile state. As in the 1D case, we analyze the linear stability of this solution. We define the operator $\mathcal{G}_1\{\delta c(x', y')\}(x, y)$ in the same way as for the 1D case. For each eigenvalue λ_i of $\mathcal{G}_1\{\delta c(x', y')\}(x, y)$, the corresponding eigenfunctions $f_{i,j}(x, y)$ introduce an irreducible representation of $O(2)$, the rotation and reflection symmetry group of the unperturbed solution. The subscript j is used to index the eigenfunctions corresponding to an eigenvalue λ_i . $O(2)$ is the group of all rotations about the origin and reflections in straight lines passing through the origin. As is generally known for the representations of $O(2)$, an eigenvalue λ_i corresponds either to a single rotationally symmetric eigenfunction

$$f_{i,1}(x, y) = f_i(r) \tag{29}$$

or to a pair of functions

$$f_{i,1}(x, y) = f_i(r) \cos m_i \phi, \quad f_{i,2}(x, y) = f_i(r) \sin m_i \phi, \tag{30}$$

where ϕ is the polar angle. Here m_i is a natural number that defines the angular dependence of the eigenfunctions $f_{i,j}(x, y)$ for given i . An explicit derivation of the form (29), (30) of the eigenfunctions is classically known for the Laplace operator ∇^2 in polar coordinates.

As in the 1D case, the derivatives $\partial_x c_0(x, y)$, $\partial_y c_0(x, y)$ are eigenfunctions of \mathcal{G}_1 with the corresponding eigenvalue equal to zero. Recall that these are translation modes. Indeed, displacing the particle and the concentration field along x or along y by constant values corresponds to neutral modes. As the activity is increased, one of the eigenvalues of the linear stability operator becomes positive at a critical activity Pe_1 and the rotationally symmetric solution becomes unstable. If this eigenvalue corresponds to eigenfunctions (30) with $m_i = 1$, the resulting solution is motile. The first unstable mode was indeed observed to have $m_i = 1$ in many models of autophoretic particles and of mammalian cell swimming [17, 21, 27, 28, 32–34].

The emerging dynamics corresponds to a self-congruent solution moving with a constant velocity along a straight line. The velocity scales as $(Pe - Pe_1)^{1/2}$. This can be demonstrated in the same way as for the 1D case. First, we assume that the concentration field is symmetric with respect to the reflection $y \rightarrow -y$. With this assumption, the perturbation of the concentration field $\delta c(x, y)$ does not contain the modes

$\partial_y c_0(x, y)$ and $f_i(r) \sin m\phi$ because they are antisymmetric with respect to the $y \rightarrow -y$ reflection. Extending the ansatz (27) to 2D then yields Eq. (28) as in the 1D case. Thus we obtain that the $y \rightarrow -y$ symmetric concentration field loses its $x \rightarrow -x$ symmetry at $Pe = Pe_1$ and the swimmer starts to move along the x direction. A question remains whether this motion is stable with respect to perturbations that do not respect the $y \rightarrow -y$ symmetry. As we show below, this solution is marginally stable for Pe sufficiently close to Pe_1 : After a perturbation without $y \rightarrow -y$ symmetry is applied, the solution relaxes to the same motion but with some shift and rotation compared to the original one.

4.2.2 Secondary bifurcation

As demonstrated in [40], the straight motion can become unstable resulting in a circular trajectory of the particle. We analyze this secondary bifurcation by reducing the dimension of the problem. First, we rewrite the evolution equation (5) in the reference frame comoving with the particle. Next, we transform the full 2D problem into a simplified 1D problem in the ϕ space for a given value of r . This would allow us to use the results of the previous section to analyze the instability.

The perturbation dynamics of the motile solution $c_1(x, y) \equiv c_1(r, \phi)$ possesses 3 soft modes (i.e. neutral modes): Two are related to translations, while the third one is related to rotation. The last mode relates to the fact that $c_1(r, \phi + \phi_0)$ is also a solution. The other perturbation modes (other than soft ones) of the $c_1(r, \phi)$ solution should correspond to negative eigenvalues for low enough values of the activity, which ensures the stability of the straight motion, as discussed below. As the activity increases, one of the perturbation modes can become unstable. The resulting dynamics can be deduced from applying the analysis developed for the 1D case to the distribution $c(r, \phi)$ as a function of ϕ for a fixed value of r . For this reason we only list schematically the main steps of the analysis. We provide in [40] an explicit calculation. The concentration field of a particle moving along the x axis possesses the $\phi \rightarrow -\phi$ (equivalently, $y \rightarrow -y$) symmetry, as discussed above. Like in 1D case, this implies that all eigenfunctions of the linear perturbation operator are either symmetric or antisymmetric with respect to the change of the sign of ϕ (equivalently, y). The secondary symmetry breaking bifurcation (loss of $y \rightarrow -y$ symmetry) occurs if the perturbation mode that loses stability is antisymmetric in y . Above the critical value Pe_2 , this mode grows exponentially until it saturates with amplitude that scales as $(Pe - Pe_2)^{1/2}$ similarly to the 1D case, provided the bifurcation is supercritical. Once the amplitude of the unstable mode reaches the steady-state value, the system follows self-congruent dynamics. Indeed, the loss of $\phi \rightarrow -\phi$ symmetry entails a self-congruent motion of the concentration field in the ϕ domain, which corresponds to the rotational soft mode of the solution $c_1(r, \phi)$. The concentration maximum drifts along the

particle periphery at a constant speed. This implies that the particle moves along a circular trajectory for $Pe > Pe_2$, as shown in Sect. 3. The angular drift velocity scales as $\omega^0 \propto (Pe - Pe_2)^{1/2}$, exactly as a drift along x -direction in 1D. The steady-state value of translational velocity is continuous at the transition point. The radius of the circle scales as $(Pe - Pe_2)^{-1/2}$ according to the analysis in Sect. 3 and the calculation in [40].

4.2.3 Perturbation spectrum

In order to provide further insight into the nature of the two bifurcations that separate the stationary phase (the non-motile solution) and the two motile phases from (the straight and circular ones) each other, we plot schematically the growth rate of the least stable eigenmodes of the stable solution (as a function of Pe in Fig. 1). We first analyze the behavior of eigenvalues in the stationary phase (the non-motile one): Each eigenvalue (except for those that correspond to rotationally symmetric modes; not shown in Fig. 1) is twofold degenerate, where the two eigenfunctions differ by \sin/\cos in the angular dependence (30). The two eigenvalues corresponding to the translation modes are exactly 0. Another branch (which is doubly degenerate, and marked $m = 1$ in Fig. 1) corresponds to the mode that becomes unstable at $Pe = Pe_1$. This branch has a negative value but increases with Pe . It reaches 0 for $Pe = Pe_1$ which corresponds to the primary bifurcation. There are thus four eigenvalues equal to 0 at $Pe = Pe_1$ (two translation modes and the twofold

degenerate $-\sin/\cos$ -branch that becomes unstable at $Pe = Pe_1$).

We now discuss how these four branches are continued into the motile phase: First, we note that the growth rate of small perturbations needs to be measured in the reference frame comoving with the unperturbed solution for the motile phases. Second, because the transition to the motile phase is continuous, the growth rate of eigenmodes evolves continuously across the transition point $Pe = Pe_1$. Third, we take the $y \rightarrow -y$ symmetric solution discussed above as the unperturbed motile solution. Our goal here is to show that the growth rate is negative for all possible perturbations of this solution, at least for some range of Pe , which would prove its stability. Since the rotational symmetry is broken in the motile phase, the eigenmodes can not be written as Eqs. (29) and (30) (which are valid only for perturbations of the fully symmetric—non-motile—solution). Nevertheless, because the unperturbed solution possesses the $y \rightarrow -y$ symmetry, the perturbation eigenmodes can be chosen to be either symmetric or antisymmetric with respect to the $y \rightarrow -y$ reflection, as was discussed in the 1D case (where we saw that eigenmodes are either symmetric or antisymmetric with respect to x). The eigenvalue branches are, in general, not degenerate in the motile phase (except for the neutral modes). This is because the x and y directions are not equivalent for a polarized concentration field. This means that each twofold degenerate branch (other than the translation branch) splits at $Pe = Pe_1$ into two simple branches. One of those branches is symmetric with respect to the $y \rightarrow -y$ reflection (continuation of the $\cos m\phi$ eigenmode in (30)), while the other one is antisymmetric (continuation of the $\sin m\phi$ eigenmode in (30)).

There are 3 neutral eigenmodes (growth rate equal to 0) for $Pe > Pe_1$: two translations and 1 rotation of the concentration field. Of these, one translation mode (along x) is symmetric with respect to $y \rightarrow -y$ reflection. The other translation mode and the rotation mode are antisymmetric with respect to $y \rightarrow -y$ reflection. The fourth mode equal to 0 at $Pe = Pe_1$ is symmetric with respect to the $y \rightarrow -y$ reflection. It corresponds to the linear stability of the non-zero solution of Eq. (28) (i.e. the mode corresponding to motility along x is stable for $Pe < Pe_2$). Its growth rate is thus negative for $Pe > Pe_1$ due to the supercritical nature of the bifurcation, as discussed in the 1D case. We thus conclude that all 4 eigenvalue branches emerging from 0 at $Pe = Pe_1$ remain non-positive for $Pe > Pe_1$. This confirms that the $y \rightarrow -y$ symmetric motile solution is marginally stable in some region above Pe_1 .

Consider now the transition from straight to circular trajectories. This transition happens at $Pe = Pe_2$ and requires a mode which is antisymmetric under the $y \rightarrow -y$ reflection to become unstable, as discussed above. This mode can not be a continuation of the $m = 1$ mode in Fig. 1 because the antisymmetric $m = 1$ mode continues as the neutral rotation mode in the motile phases. We therefore conclude that the instability occurs due to another mode, the growth rate of

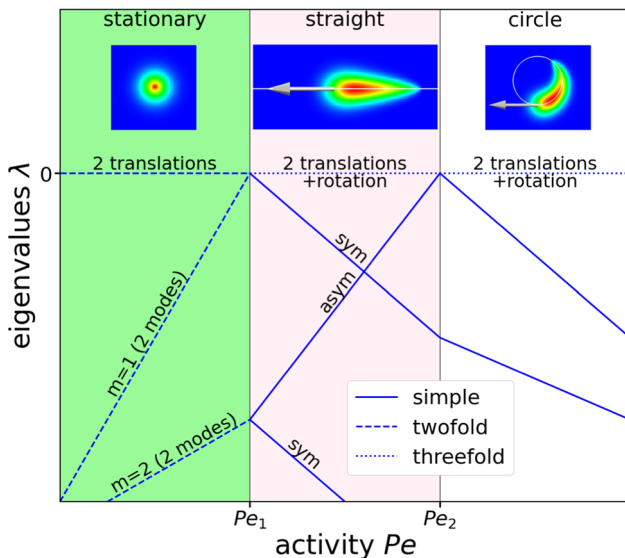


Fig. 1 Schematic view of the growth rate of the most unstable modes as a function of the activity. The modes symmetric and antisymmetric with respect to the $y \rightarrow -y$ reflection are marked as sym and asym, respectively. Insets show the characteristic dynamics of the particle in each phase. Color code shows the concentration distribution. Arrows show the velocity of motile particles. White curves show the trajectories

which is negative for the stationary and straight phases but increases reaching zero at $Pe = Pe_2$. It is shown in [40] that including the first two harmonics ($m_i = 1, 2$ in Eq. (30) in the concentration field is sufficient to observe both the primary and the secondary instability. For this reason, we have marked the mode that loses stability at $Pe = Pe_2$ as $m = 2$ mode, which is a natural choice but not a general rule.

We plot the growth rate of the perturbation eigenmodes for the circular trajectory for $Pe > Pe_2$. Since this solution does not satisfy any spatial symmetry, neither do the corresponding perturbation modes. The continuation of the antisymmetric $m = 2$ mode has a negative growth rate for $Pe > Pe_2$ as is expected for a linearly stable state.

4.3 3D case: spherical particle in a space

Here we provide a brief description of the 3D case. An explicit model showing the bifurcations presented here is analyzed in detail in the next Section. The bifurcation sequence in 3D space follows the pattern described for 1D and 2D. It is convenient to relate the angular dependence of the concentration field in 3D to that in 2D, as shown in Fig. 2. For low enough Pe the concentration field has the full rotational symmetry, which corresponds to a homogeneous concentration in 2D (Fig. 2, column A). The angular dependence of a given perturbation mode in 3D corresponds to a spherical harmonic of some degree. All perturbations decay for low enough activity and the system is stationary in this case. The spherical symmetry is broken at a critical activity Pe_1 . If the angular dependence of the mode that becomes unstable at $Pe = Pe_1$ corresponds to the first spherical harmonic, the bifurcation results in a motile self-congruent solution. A circular spot of concentration appears in the angular dependence, which corresponds to a stationary axisymmetric concentra-

tion field in 2D (Fig. 2, column B). The 3D particle moves along a fixed direction defined by the orientation of the spot (where the 2D analogue corresponds to a non motile solution). The norm of the velocity scales as $(Pe - Pe_1)^{1/2}$ close to the transition point. According to the 2D analysis, the concentration spot loses its axial symmetry and moves along a straight line at $Pe = Pe_2$. The spherical counterpart of this effect is a non-circular spot of concentration moving along the equator (Fig. 2, column C). This corresponds to the case when the angular velocity of the corotational frame is orthogonal to the translational velocity, meaning that the particle moves along a circle. The radius of the circle scales as $(Pe - Pe_2)^{-1/2}$ close to the transition point. Finally, this solution becomes unstable with respect to the loss of the remaining mirror symmetry at $Pe = Pe_3$. In 2D, the concentration spot moves along the particle periphery, corresponding to a circular path for the particle. In 3D this corresponds to a concentration spot moving along a small circle (i.e. a circle outside the equator; Fig. 2, column D). The 3D trajectory is a helix in this case. The pitch of the helix scales as $(Pe - Pe_3)^{1/2}$ close to the transition point.

5 Example: a simple exactly solvable model

5.1 Model formulation

The above analysis shows how a helical trajectory can appear after a series of symmetry-breaking bifurcations for an isotropic motile particle. The question however remains whether this series of bifurcations can be actually realized in practice. To show that this is indeed the case, we constructed an exactly solvable model which manifests the desired trajectory types. The model is taken as simple as possible and thus relies only on two harmonics of the concentration field, the first harmonic c_i and the second one c_{ij} . Here c_i is a 3D vector and c_{ij} is a 3D symmetric traceless tensor. This Cartesian representation turns out to simplify notations in comparison to use of spherical coordinates. The particle is taken as a unit sphere with a concentration field distributed on its surface. The concentration field at point \mathbf{r} on the sphere is given by

$$c(\mathbf{r}, t) = c_i(t)r_i + c_{ij}(t)r_i r_j. \tag{31}$$

Note that both $c_i(t)$ and $c_{ij}(t)$ in (31) are functions of time only. The angular dependence of the concentration field is given explicitly by the components of \mathbf{r} in (31). For simplicity, the time dependence of c_i and c_{ij} is implied below. We propose the following dynamics equations:

$$\dot{c}_i = \sigma_1 c_i + \alpha_1 c_j^2 c_i + \beta_1 (c_k^2 c_{ij} c_j - c_j c_k c_{jk} c_i) \tag{32a}$$

$$\dot{c}_{ij} = \sigma_2 c_{ij} + \beta_2 (c_i c_j - \delta_{ij} c_k^2 / 3), \tag{32b}$$


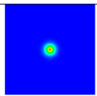
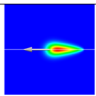
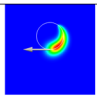

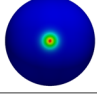
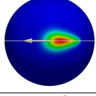
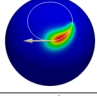
column tag	A	B	C	D
concentration in 2D				
concentration on a sphere in 3D				
trajectory in 2D	–	stationary	straight	circle
locus of velocity orientations in 3D	–	stationary	great circle	small circle
trajectory in 3D	stationary	straight	circle	helix

Fig. 2 Analogy between the types of self-congruent solutions on a plane in 2D and the angular dependence of the types of self-congruent solutions in 3D. Color code represents the concentration field. White curves of the concentration field and arrows in columns C and D show the time evolution of the system: The white curves show the trajectory of the concentration maximum (in comoving frame for the spherical case). The white arrows show the instantaneous motion of the concentration maximum

where δ_{ij} is the identity matrix. We choose the propulsion velocity $\mathbf{v}(t)$ of the particle as $v_i = c_i$. As explained in [40] whenever the velocity is a linear function of concentration (and/or of derivatives of c), the component of the swimming velocity, v_i , is linear in c_i (first harmonic component). The above equations are based on symmetry as they are invariant under rotations of the coordinate system. The particular form of the last term of Eq. (32a) is chosen in such a way that the equation for the amplitude of c_i be independent of c_{ij} to simplify the symbolic analysis. This can easily be checked by multiplying the first equation by c_i . The next Section presents a more generic model, which we analyze numerically with qualitatively the same results. Note that recently we have mapped [41] the full phoretic model on a two-mode set of equations in two dimensions similar to Eqs. (32a, 32b). The same mapping can be performed in three dimensions.

As we show below, the system (32a, 32b) possesses the desired properties:

- Its solutions can be found analytically.
- The stable solution goes from no motion to straight motion to circular motion to helical motion when σ_1 is increased and the other parameters are fixed. In other words, self-congruent solutions emerge naturally.

5.2 Primary bifurcation

The key to understanding the system (32a, 32b) lies in the fact that the β_1 term in Eq. (32a) is orthogonal to c_i . This leaves the evolution of the norm of c_i independent of c_{ij} :

$$c_i \dot{c}_i = \sigma_1 c_i^2 + \alpha_1 (c_i^2)^2. \tag{33}$$

This is the classical form of a pitchfork bifurcation. We choose $\alpha_1 < 0$ in order to ascertain a supercritical bifurcation. With this choice, we obtain that for $\sigma_1 < 0$ the stable solution is $c_i^2 = 0$, which corresponds to a non-motile case. For $\sigma_1 > 0$, the stable solution is

$$c_i^2 = -\sigma_1 / \alpha_1, \tag{34}$$

which corresponds to a motile solution. Since the norm dynamics of c_i is intrinsic (independent of c_{ij}), we assume below that the norm of c_i has already reached its stationary value defined by Eq. (34). The exact form of the motile solution depends only on the orientational dynamics of c_i .

As we have seen before for a self-congruent solution the concentration field is stationary in a given frame (to be determined) which is related to the laboratory frame by a rigid translation and rotation. For this reason we find it more convenient to rewrite the equations in the frame co-rotating with c_i . We call $\boldsymbol{\omega}$ the angular velocity (unknown for the moment) of the coordinate system which would keep the orientation of c_i fixed. In the corotating frame the time derivative transforms as:

$$\dot{c}(\mathbf{r}) \rightarrow \dot{c}(\mathbf{r}) - [\boldsymbol{\omega} \times \mathbf{r}] \cdot \nabla^s c(\mathbf{r}), \tag{35}$$

where ∇^s is the surface gradient operator on the sphere. Here $-\boldsymbol{\omega} \times \mathbf{r}$ is the velocity field on the sphere measured in the corrotational frame.

Equation (35) defines the change of equations (32a, 32b) when going in the corrotational frame:

$$\dot{c}_i + \epsilon_{ijk} \omega_j c_k = \sigma_1 c_i + \alpha_1 c_j^2 c_i + \beta_1 (c_k^2 c_{ij} c_j - c_j c_k c_{jk} c_i) \tag{36a}$$

$$\dot{c}_{ij} + \epsilon_{ikl} \omega_k c_{lj} + \epsilon_{jkl} \omega_k c_{li} = \sigma_2 c_{ij} + \beta_2 (c_i c_j - \delta_{ij} c_k^2 / 3). \tag{36b}$$

Setting the angular velocity to

$$\boldsymbol{\omega}_i = \beta_1 \epsilon_{ijk} c_j c_{kl} c_l + \mu c_i \tag{37}$$

cancels the β_1 term in Eq. (36a). Here μ is a constant, the value of which does not affect \dot{c}_i in Eq. (36a). This happens because the vector c_i remains invariant on any rotation about its direction. We choose μ to cancel the rotation of c_{ij} about c_i , as explained below. This implies that μ is set to 0 except when dealing with the helical case.

The choice (37) makes Eq. (36a) trivial. This reduces the analysis of the rotational dynamics of c_i to the study of Eq. (36b), where $\boldsymbol{\omega}$ and $|c_i|$ are defined by Eqs. (34) and (37), respectively. We choose the direction of c_i as the x axis in the co-rotational frame.

5.3 Secondary bifurcation

We saw above that if only the first harmonic c_i is taken into account then there is a supercritical bifurcation from non-motile to a motile state (when $\sigma_1 > 0$; see Eq. (34)). This is referred to as the primary bifurcation. The question we answer below is whether or not the system shows other types of trajectory (circular, helical), and if so under which conditions. The circular solution results from the loss of stability of the straight solution, and we refer to this situation as the secondary bifurcation.

It is clear from (37) that the occurrence of a non-zero rotation of c_i requires a coupling between first and second harmonics. It is geometrically clear that if the direction of c_i is taken as the x axis in the co-rotational frame, then a circular trajectory corresponds to $\boldsymbol{\omega}$ being orthogonal to x axis. For example, if $\boldsymbol{\omega}$ is along z , this means that c_i moves along the equator in the x, y plane in the lab frame. The occurrence of non-zero $\boldsymbol{\omega}$ depends on symmetry of c_{ij} , as seen below.

The remaining procedure is the following: we first restrict the stationary solutions of c_{ij} to the ones which respect a plane of symmetry, which corresponds to circular trajectories. Then we analyze the linear stability of these solutions with respect to the loss of the mirror symmetry, which yields the transition point to the helical trajectories. Finally, we relax the mirror symmetry in order to find the analytical expressions for the helical solutions.

Assuming the tensor c_{ij} to be symmetric with respect to the (x, y) plane, we can set c_{xz} and c_{yz} to 0. Because

ω is orthogonal to c_i , we set μ in Eq. (37) to 0. The only non-zero component of the angular velocity is ω_z in this case, given by

$$\omega_z = \beta_1 c_i^2 c_{xy} \tag{38}$$

Using (36b) and (38) yields the following equations for the diagonal terms:

$$\dot{c}_{xx} = \sigma_2 c_{xx} + 2\beta_1 c_i^2 c_{xy}^2 + \frac{2\beta_2 c_i^2}{3}, \tag{39a}$$

$$\dot{c}_{yy} = \sigma_2 c_{yy} - 2\beta_1 c_i^2 c_{xy}^2 - \frac{\beta_2 c_i^2}{3}. \tag{39b}$$

The \dot{c}_{zz} equation is linearly dependent on set (39a, 39b) by virtue of the zero-trace property of c_{ij} . Choosing σ_2 to be negative is necessary to ensure linear stability of c_{ij} described by Eqs. (39a, 39b). Setting $\dot{c}_{xx} = \dot{c}_{yy} = 0$ yields the expressions for c_{xx} and c_{yy} as functions of c_{xy} . These expressions are substituted into the \dot{c}_{xy} equation to provide

$$\dot{c}_{xy} = \left(\frac{\beta_1 \beta_2 (c_i^2)^2}{\sigma_2} + \sigma_2 \right) c_{xy} + \frac{4\beta_1^2 (c_i^2)^2}{\sigma_2} c_{xy}^3. \tag{40}$$

Equation (40) corresponds to a pitchfork bifurcation, which is of supercritical type because the coefficient of the cubic term is negative for $\sigma_2 < 0$. The coefficient of the linear term is negative for $c_i^2 = 0$ but can change its sign for large enough c_i^2 , provided $\beta_1 \beta_2 < 0$. For $\beta_1 \beta_2 (c_i^2)^2 < \sigma_2^2$, the stable solution is $c_{xy} = 0$, which corresponds to an axisymmetric solution $c_{yy} = c_{zz} = -c_{xx}/2$. The angular velocity is zero in this case and the particle moves along a straight line. For $\beta_1 \beta_2 (c_i^2)^2 > \sigma_2^2$, the stable solution is

$$c_{xy}^2 = -\frac{\beta_2}{4\beta_1} - \frac{\sigma_2^2}{4\beta_1^2 (c_i^2)^2}, \tag{41}$$

which corresponds to non-zero ω . This results in the concentration field rotating in the laboratory frame with angular velocity orthogonal to the propulsion velocity and defined by Eqs. (38) and (41). The trajectory is a circle in this case. Indeed, the propulsion velocity $v_i = c_i$ is directed along x and the rotation speed is along z in the corotating frame. This means that the propulsion velocity in the laboratory frame rotates along the equator contained in the plane (x, y) with pulsation ω_z . It has thus two components $v_x \sim \sin(\omega_z t)$ and $v_y \sim \cos(\omega_z t)$, and the corresponding trajectory behaves as $x \sim \cos(\omega_z t)/\omega_z$ and $y \sim \sin(\omega_z t)/\omega_z$, which is a circle with radius proportional to ω_z^{-1} . According to (38) ω_z is proportional to c_{xy} , which vanishes as the square root of the distance from the bifurcation point (defined by right hand side of Eq. (41) equal to zero). This means that the circle radius diverges with square root singularity at the bifurcation point, as we find from our general consideration and explicitly in 2D in [40].

5.4 Tertiary bifurcation

Now let us analyze the linear stability of the non-trivial solution of Eq. (40), which has led to a circular trajectory, with respect to the loss of the mirror symmetry. Recall that circular solution emerges at the secondary bifurcation. The loss of stability of the circular solution corresponds to a tertiary bifurcation. A helical solution emerges at this point as shown below. The circular solution corresponds to $c_{yz} = c_{xz} = 0$ (mirror symmetry with respect to (x, y) plane). The occurrence of a non-zero value of c_{yz} or c_{xz} breaks this symmetry and leads to a new trajectory. The evolution equations for the xz and yz components of c_{ij} in the corotating frame read (from Eq. (36b) with $\mu = 0$)

$$\dot{c}_{xz} = \sigma_2 c_{xz} + \beta_1 c_i^2 (c_{xy} c_{yz} + c_{xz} c_{yy} + 2c_{xz} c_{zz}) \tag{42a}$$

$$\dot{c}_{yz} = \sigma_2 c_{yz} - 2\beta_1 c_i^2 c_{xy} c_{xz}. \tag{42b}$$

Substituting the steady-state values of c_{yy} , c_{zz} , and c_{xy} , we get that the determinant of the linear stability matrix is always zero. This means that one of the eigenvalues of the linear stability matrix is zero. This eigenvalue corresponds to the rotation of the problem about the c_i direction. Since one of the eigenvalues is zero, the trace of the linear stability matrix is equal to the second eigenvalue. We therefore use the trace of the linear stability matrix of the system (42a, 42b) to analyze the stability of the circular motion:

$$\frac{\partial \dot{c}_{xz}}{\partial c_{xz}} + \frac{\partial \dot{c}_{yz}}{\partial c_{yz}} = 2\sigma_2 + \beta_1 c_i^2 (c_{yy} + 2c_{zz}) = \frac{\beta_1 \beta_2 (c_i^2)^2}{2\sigma_2} + \frac{3\sigma_2}{2}, \tag{43}$$

where the last equality is obtained by substituting the steady-state values of c_{yy} and c_{zz} . The circular motion thus becomes unstable for $(c_i^2)^2 > 3\sigma_2^2/(\beta_1 \beta_2)$, which happens when c_i^2 (or, equivalently, σ_1) exceeds a critical value.

It is possible to calculate the rotational velocity ω analytically even without assumption of the $z \rightarrow -z$ symmetry of c_{ij} . This is done by choosing the value of μ (setting ω_x in the corotating frame) in Eq. (37) in such a way that $\dot{c}_{xz} = 0$ in Eq. (36b). Without loss of generality, we choose the z axis such that $c_{xz} = 0$. The loss of $z \rightarrow -z$ symmetry is manifested as $c_{yz} \neq 0$ in this case. The value of ω_x is given by

$$\omega_x = -\beta_1 c_i^2 c_{yz}. \tag{44}$$

The evolution equation for c_{yz} reads

$$\dot{c}_{yz} = c_{yz} [\sigma_2 - \beta_1 c_i^2 (c_{yy} - c_{zz})]. \tag{45}$$

Equation (45) shows two possibilities for fixed points: $c_{yz} = 0$, which corresponds to the $z \rightarrow -z$ symmetric solution considered above in Sect. 5.3 and a new possibility

$$c_{yy} - c_{zz} = \frac{\sigma_2}{\beta_1 c_i^2}. \tag{46}$$

Exploring this possibility yields

$$c_{yz}^2 = -\frac{\beta_2}{6\beta_1} - \frac{\sigma_2^2}{2\beta_1^2(c_i^2)^2}, \tag{47}$$

where both signs of c_{yz} are possible. We also give the value c_{xy} for the $c_{yz} \neq 0$ fixed point, which is necessary to evaluate the ω_z component of the angular velocity:

$$c_{xy}^2 = -\frac{\beta_2}{3\beta_1} - \frac{\sigma_2^2}{2\beta_1^2(c_i^2)^2}. \tag{48}$$

The solution defined by Eqs. (47) and (48) corresponds to helical motion according to the analysis in Sect. 3. Indeed, due to non-zero c_{yz} , $\omega_x^0 \neq 0$, which implies that ω^0 and v^0 be not orthogonal. The pitch of the helix is defined by Eq. (19). The trajectories of the particle and the corresponding concentration fields can be obtained numerically, as shown in the next Section for a slightly different model.

5.5 Bifurcation diagram

The following assumptions were used to obtain all 3 possible bifurcations:

- $\sigma_2 < 0$
- $\beta_1\beta_2 < 0$
- $\alpha_1 < 0$

These assumptions guarantee that all bifurcations are of supercritical pitchfork type. The final expressions for the translational and rotational velocities of the comoving and corotating frame read

$$v^0 = \begin{cases} 0 & \text{for } \sigma_1 \leq 0 \\ \sqrt{-\frac{\sigma_1}{\alpha_1}} & \text{for } \sigma_1 > 0, \end{cases} \tag{49}$$

$$\omega_{\perp}^0 = \begin{cases} 0 & \text{for } \sigma_1 \leq \frac{\alpha_1\sigma_2}{\sqrt{-\beta_1\beta_2}} \\ \sqrt{-\frac{\sigma_2^2}{4} - \frac{\beta_1\beta_2\sigma_1^2}{4\alpha_1^2}} & \text{for } \frac{\alpha_1\sigma_2}{\sqrt{-\beta_1\beta_2}} < \sigma_1 < \frac{\alpha_1\sigma_2\sqrt{3}}{\sqrt{-\beta_1\beta_2}} \\ \sqrt{-\frac{\sigma_2^2}{2} - \frac{\beta_1\beta_2\sigma_1^2}{3\alpha_1^2}} & \text{for } \sigma_1 > \frac{\alpha_1\sigma_2\sqrt{3}}{\sqrt{-\beta_1\beta_2}}, \end{cases} \tag{50}$$

$$\omega_{\parallel}^0 = \begin{cases} 0 & \text{for } \sigma_1 \leq \frac{\alpha_1\sigma_2\sqrt{3}}{\sqrt{-\beta_1\beta_2}} \\ \sqrt{-\frac{\sigma_2^2}{2} - \frac{\beta_1\beta_2\sigma_1^2}{6\alpha_1^2}} & \text{for } \sigma_1 > \frac{\alpha_1\sigma_2\sqrt{3}}{\sqrt{-\beta_1\beta_2}}, \end{cases} \tag{51}$$

where ω_{\perp}^0 and ω_{\parallel}^0 are the components of the ω^0 perpendicular and parallel to v^0 , respectively. As shown in Sect. 3, the case $v^0 = 0, \omega^0 = 0$ corresponds to a stationary particle, the case $v^0 > 0, \omega^0 = 0$ corresponds to straight motion, the case $v^0 > 0, \omega_{\perp}^0 > 0, \omega_{\parallel}^0 = 0$ corresponds to a circular motion and the case $v^0 > 0, \omega_{\perp}^0 > 0, \omega_{\parallel}^0 > 0$ corresponds to a helical motion.

Figure 3 shows expressions (49), (50) and (51) plotted as functions of σ_1 . We use direct numerical simulations

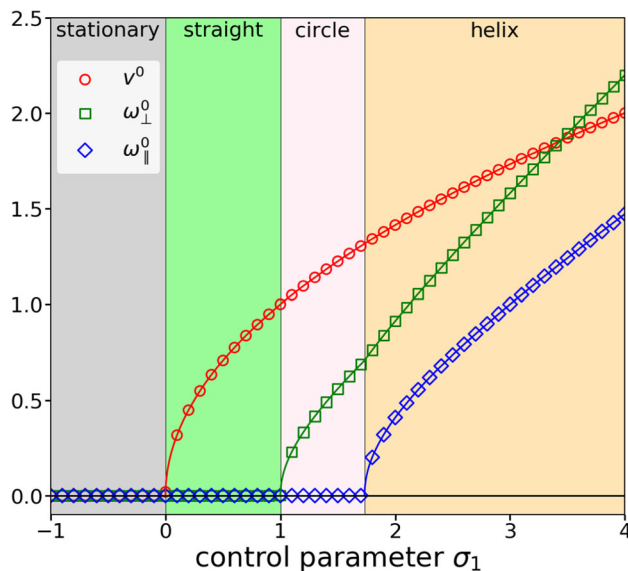


Fig. 3 Saturation values of velocity v^0 and angular velocity ω^0 of the comoving and corotating reference frame for a self-propelling particle described by Eqs. (32a, 32b). The components of angular velocity along the velocity and orthogonal to it are shown as ω_{\parallel}^0 and ω_{\perp}^0 , respectively. $\sigma_2 = -1, \alpha_1 = -1, \beta_1 = 1, \beta_2 = -1$. Symbols are full numerical solution of equations (32a, 32b). Solid lines are analytical expressions. The color regions denote the trajectory type

of Eqs. (32a, 32b) to validate the analytical results. The details of the numerical procedure are given in the next section. As can be seen, the analytical results match the numerical simulations exactly. This confirms that the full dynamics of the system (32a, 32b) relaxes to the appropriate self-congruent solution for the explored parameters.

We summarize the results in a table (Table 1), showing the symmetry of the concentration field, the trajectory, and the concentration dynamics for different σ_1 .

6 Direct numerical solution

Section 5 deals with a system of equations (system (32a, 32b)) which has a special property: the evolution of c_i^2 is completely decoupled from the rest of the dynamics. We show here that c_i^2 relaxes to a time-independent value even if it is coupled to c_{ij} and the orientation of c_i . To highlight the genericity of the presented results, we write below (as we did in 2D [40]) the evolution equations for the first and second harmonics based on symmetry only (invariance under 3D rotations). To the leading order we have

$$\dot{c}_i = \sigma_1 c_i + \alpha_1 c_j^2 c_i + \beta_1 c_{ij} c_j \tag{52a}$$

$$\dot{c}_{ij} = \sigma_2 c_{ij} + \beta_2 (c_i c_j - \delta_{ij} c_k^2 / 3). \tag{52b}$$

Table 1 Types of particle dynamics for different values of σ_1

σ_1 Range	Concentration symmetry	Concentration maximum trajectory	Trajectory
$\sigma_1 < 0$	$O(3)$ (spherical)	–	Stationary
$0 < \sigma_1 < \frac{\alpha_1 \sigma_2}{\sqrt{-\beta_1 \beta_2}}$	$C_{\infty v}$ (axial+mirror)	Stationary	Straight
$\frac{\alpha_1 \sigma_2}{\sqrt{-\beta_1 \beta_2}} < \sigma_1 < \frac{\alpha_1 \sigma_2 \sqrt{3}}{\sqrt{-\beta_1 \beta_2}}$	C_s (mirror)	Great circle (equator)	Circle
$\frac{\alpha_1 \sigma_2 \sqrt{3}}{\sqrt{-\beta_1 \beta_2}} < \sigma_1$	C_1 (trivial)	Small circle	Helix

Solving the differential equations (52a, 52b) for given values of parameters yields the functions $c_i(t)$ and $c_{ij}(t)$. The following procedure is used to extract the values ω_{\perp}^0 , and ω_{\parallel}^0 . We define 3 mutually orthogonal unit vectors e^1, e^2 , and e^3 , corotating with the concentration field:

$$e_i^1 = \frac{c_i}{|c_i|}, \tag{53a}$$

$$e^2 = \frac{e^1 \times b}{|e^1 \times b|}, \text{ where } b_i = c_{ij}c_j, \tag{53b}$$

$$e^3 = e^1 \times e^2. \tag{53c}$$

There are situations in which the vector e^2 is ill-defined, meaning that the vector $b_i = c_{ij}c_j$ is parallel to c_i . This only happens when the trajectory is not helical and we can set effectively ω_{\parallel} to 0 in this case. The time derivatives of vectors e^i define the rotation of the concentration field. Indeed, it is evident that a simultaneous rotation of c_i and c_{ij} leads to the same rotation of e^i . The vectors e^k with $k \in \{1, 2, 3\}$ satisfy the evolution equations $\dot{e}^k = \omega \times e^k$ for purely rotational dynamics. This implies that

$$\sum_{k=1}^3 (\dot{e}^k)^2 = \sum_{k=1}^3 [\omega^2 (e^k)^2 - (e^k \cdot \omega)^2] = 2\omega^2, \tag{54}$$

where we have used that the vectors e^k form an orthonormal basis. Hence we compute the angular velocities as

$$\omega_{\perp} = |\dot{e}^1|, \quad \omega_{\parallel} = \sqrt{\frac{(\dot{e}^2)^2 + (\dot{e}^3)^2 - (\dot{e}^1)^2}{2}}, \tag{55}$$

using that e^1 is parallel to c_i .

First we show that the velocity and angular velocity of the comoving and corotating frame tend to a fixed value after the initial transients have decayed. The results are presented in Fig. 4 for a given set of parameters corresponding to the helical phase. As can be seen, the system tends to a self-congruent dynamics after an initial transient. v_0 is given by the amplitude of c (first harmonic), and we see that after transients the amplitude tends to a constant, meaning that the choice of the exactly solvable model (32a, 32b) (where we assumed c_i^2 is conserved) was legitimate.

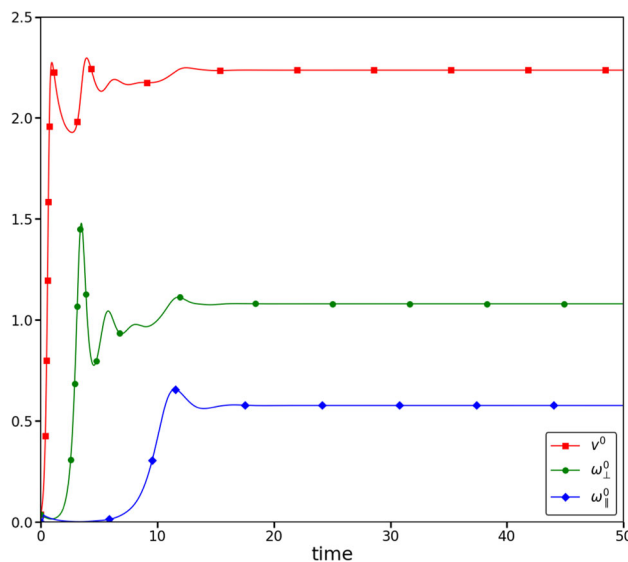


Fig. 4 Velocity v^0 and angular velocity ω^0 of the comoving and corotating reference frame for a self-propelling particle described by Eqs. (52a, 52b) as a function of time. The components of angular velocity along the velocity and orthogonal to it are shown as ω_{\parallel}^0 and ω_{\perp}^0 , respectively. $\sigma_1 = 6$, $\sigma_2 = -1$, $\alpha_1 = -1$, $\beta_1 = 1$, $\beta_2 = -1$. Solid lines are full numerical solution of equations (52a, 52b). Symbols have no special meaning other than helping to distinguish the curves

Next, we plot the saturation values of $v^0, \omega_{\parallel}^0$, and ω_{\perp}^0 as functions of σ_1 . The results are shown in Fig. 5. As can be seen, the bifurcation diagram is similar to the one discussed in the previous Section (Fig. 3).

We use the numerical solutions $c_i(t)$ and $c_{ij}(t)$ to plot the dynamics of the concentration field (defined by Eq. (31)) and the trajectories of the particle in 3D, as shown in Fig. 6. The non-motile solution is characterized by zero concentration field (not shown in Fig. 6). The concentration field for straight motion has an axisymmetric spot of high concentration, the orientation of which remains constant with respect to the particle center. Left panel of Fig. 6 shows the concentration field for the case of circular trajectory. As can be seen, the concentration field is symmetric with respect to a plane passing through the center of the particle. The rotation of the concentration field is such that the center of the high-concentration spot (which corresponds to the orientation of the particle velocity) moves along the equator (white curve on the particle surface).

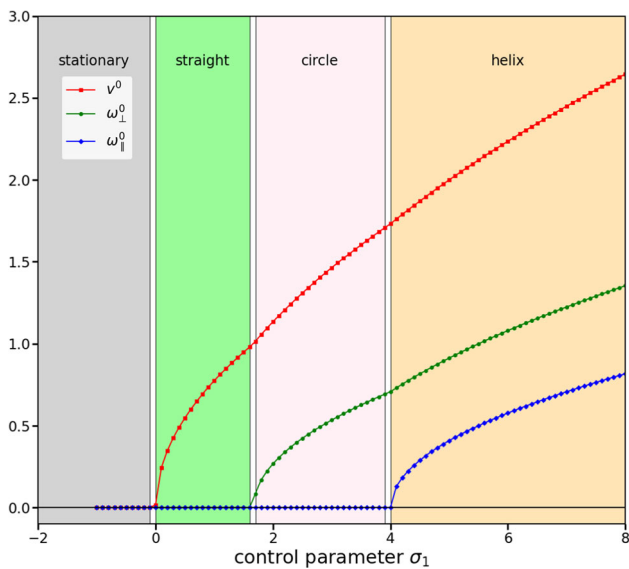


Fig. 5 Velocity v^0 and angular velocity ω^0 of the comoving and corotating reference frame for a self-propelling particle described by Eqs. (52a, 52b). The components of angular velocity along the velocity and orthogonal to it are shown as ω_{\parallel}^0 and ω_{\perp}^0 , respectively. $\sigma_2 = -1$, $\alpha_1 = -1$, $\beta_1 = 1$, $\beta_2 = -1$. Solid lines are full numerical solution of equations (52a, 52b). The color regions denote the trajectory type. Symbols have no special meaning other than helping to distinguish the curves

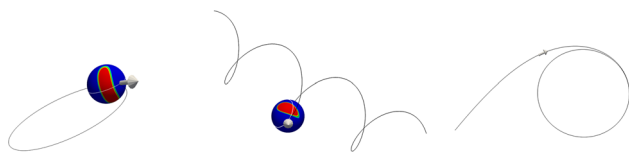


Fig. 6 Characteristic concentration distributions and particle trajectories. Time-dependent solutions of Eqs. (52a, 52b). $\sigma_2 = -1$, $\alpha_1 = -1$, $\beta_1 = 1$, $\beta_2 = -1$. Left: circular trajectory $\sigma_1 = 3$, Center: helical trajectory $\sigma_1 = 5$, Right: transient trajectory from straight to circular motion $\sigma_1 = 2$. Color code: concentration field, black curve: particle trajectory, white curve on particle surface: locus of velocity orientations, arrow: instantaneous velocity. The color code is scaled in a way that highlights the spot of high concentration

For the helical case (central panel of Fig. 6), the spot of high concentration is not symmetric and rotates in such a way that the velocity direction follows a closed loop corresponding to a small circle on the particle surface. Finally we also present the transient behavior of the system, when the particle initially starts to move along a straight line until the symmetry breaking instability develops and the trajectory becomes circular (right panel of Fig. 6). This corresponds to growth of ω^0 from 0 to its saturation value, while v^0 remains close to a constant and orthogonal to ω^0 . We can see that the trajectory spirals in to the circle in this case.

7 Discussion

The presented analysis shows that straight, circular, and helical trajectories in systems powered by a concentration field (like phoretic systems, and motile systems assisted by acto-myosin kinetics) belong to a general class of self-congruent solutions and can emerge through a series of pitchfork bifurcations from a stationary solution. Our model is very general and relies on the motility of the particle being related to a concentration field which can be distributed on the particle surface and/or in the media inside or outside it. The shape of the particle is taken rotationally invariant and the breaking of the rotational symmetry of the system occurs spontaneously in the concentration field as the particle activity is increased. An important feature of our model is that the position of the particle and its propulsion velocity are incorporated implicitly, similarly to the phase-field models. That is, the model applies as long as the shape or position of the particle are not independent but are a function of the concentration field. This is true, for example, even for deformable particles, as long as the shape relaxation is fast enough for adiabatic elimination to make sense. Furthermore, the particle does not need to be a physical entity and the model pertains as well to soliton-like solutions when concentration peaks move in a homogeneous medium.

This generality of the model makes it applicable for a very diverse set of physical situations: The prototypical example is an autophoretic droplet [16, 17, 19, 21]. Another example is the model of cell motility, where the activity is driven by myosin motors distributed in the cortex along the surface of a spherical cell and/or inside it [32–34]. Our model is still applicable if the cell is not spherical, as long as the shape of the cell can be reconstructed from the concentration field and is a sphere for low enough motility. Another example is the dynamics of myosin concentration in tissues, where our model can be used to describe the motion of localized concentration peaks [35, 36].

This study considers the case when the symmetry breaking occurs by a steady pitchfork bifurcation. We considered the case of supercritical bifurcation when the solution changes continuously at the critical point. The transition is discontinuous for subcritical bifurcations. In this case, it is generally not possible to predict the properties of the motile solutions by analyzing the dynamics close to the non-motile branch. However, for a weakly subcritical bifurcation, a systematic analysis similar to the present one can be adopted.

Another possibility is Hopf bifurcation. The solutions show periodic oscillations in this case. For example, a 1D phoretic system undergoing Hopf bifurcation would show a back-and-forth motion of the particle. The oscillations can arise due to a strong coupling of two different spatial modes. Another possibility is coupling between concentration dynamics of two chemical species, such as actin and myosin [34]. In 2D, Hopf bifurcation can happen either as the primary (translational modes) or the secondary (angu-

lar) instability. There are two translational degrees of freedom in 2D, which are both excited in the case of the primary bifurcation. The non-linear terms set the interaction between the oscillations along two orthogonal directions. There are two possible solutions in this case, which correspond to planar and circular polarization. The first case is similar to the 1D situation with back-and-forth motion of the particle, while the second case shows circular trajectories. The radius of the circle grows continuously from zero at the instability point in this case. Hopf bifurcation as the secondary instability leads to periodic oscillations of the velocity orientation, which leads to meandering [16]. It is hoped to investigate this matter in the future.

Here we have considered that the spectrum is discrete, meaning that the system size is finite (albeit arbitrary large). For a phoretic model [22] it has been reported recently that for an infinite system size, close to the bifurcation point from a nonmotile to a motile state, the velocity behaves as $v^0 \sim Pe - Pe_1$, and not as $(Pe - Pe_1)^{1/2}$, as we found above. This result is confirmed by Saha et al. [42]. Actually this finding was also reported earlier by Rednikov et al. [27] (see their equation 24). To be more precise $|v^0| \sim Pe - Pe_1$, and the absolute value is a signature of singular behavior. The result $|v^0| \sim Pe - Pe_1$ implies the existence of two symmetric branches of solutions $v^0 \sim \pm(Pe - Pe_1)$, and the bifurcation is not transcritical, as stated in [22], but of pitchfork (albeit singular) nature. In simulations [16] the size is finite and $v^0 \sim (Pe - Pe_1)^{1/2}$ (pitchfork bifurcation). We have recently discussed [43] how the singular bifurcation can be regularized (due, in particular, to a finite size) into a classical pitchfork bifurcation. Since secondary bifurcations during transition to circular or helical motions occur in the angular domain, which corresponds either to a sphere or a circle, these secondary bifurcations are always regular.

Our study shows that the primary instability corresponds to a transition from a steady to a motile state with a straight trajectory. That is, there is no possibility to go from a fully isotropic concentration distribution to a state with $v^0 = 0$ and $\omega^0 \neq 0$. This is because the rotational invariance of the concentration field needs to be broken first for solutions with time-dependent angular dependence to make sense. Spiral-like trajectories have been observed in experiments. A logarithmic spiral corresponds to a constant value of $\omega(t)$ and the amplitude of $v(t)$ that grows exponentially. This suggests that spiral-like trajectories can not appear as a transient for a steady pitchfork bifurcation but can for Hopf bifurcation. Detailed analysis of Hopf bifurcations in phoretic systems and finding a simple model which shows such behavior is thus a promising topic for future research.

Finally, the dynamics of a phoretic system does not necessarily relax to a self-congruent solution. As the 2D studies show [16, 40], periodic oscillations of strongly anharmonic form or even chaotic dynamics are among the possible solutions. Investigating the 3D analogs of those types of dynamics represents another problem for future research.

Acknowledgements We are grateful to Romy Morin for correcting several equations in the early version of the manuscript. We thank CNES (Centre National d'Etudes Spatiales) (C.M. and A.F.) and the French-German university program "Living Fluids" (grant CFDA-Q1-14) (C.M., A.F. and S.R.). The computations presented in this paper were performed using the GRICAD infrastructure (<https://gricad.univ-grenoble-alpes.fr>), which is supported by Grenoble research communities.

Author contribution statement

AF did most of calculation, SR made preliminary 2D calculation (not shown here), W-FH and TSL did numerical simulations of full model that identified many interesting features, SR helped to analyze the results, C.M. proposed the 2D model (not shown here) that inspired the 3D explicit model. A.F. and C.M. designed the research plans. All authors contributed to the writing of the article.

Data availability No Data associated in the manuscript.

Declarations

Conflict of interest The authors have no conflict of interest.

Appendix A: Explicit model: autophoretic particle in 2D

Let us consider an explicit model studied in [16, 17, 19, 21]. This is an autophoretic particle which can emit (or absorb) a chemical substance at its surface. In that case the tangential velocity field along the particle is related to the surface gradient of the chemical concentration. The flow equations can be solved for to express the fluid velocity in terms of the concentration field at the particle surface. The concentration dynamics in the bulk, which obeys an advection–diffusion equation, defines a nonlinear evolution equation for the concentration in the bulk and at the surface [16, 17, 19, 21]. For example, the evolution equation reads

$$\begin{aligned} \dot{c}(\mathbf{r}, t) &= \sum_k \frac{c_k(1, t) M e^{ik\phi}}{2r^{|k|+1}} \\ &\left[(r^2 - 1)k^2 \frac{\partial c(\mathbf{r}, t)}{\partial r} + ik(2r^2 + (1 - r^2)|k|) \frac{\partial c(\mathbf{r}, t)}{\partial \phi} \right] \\ &+ \frac{1}{Pe} \Delta c(\mathbf{r}, t) \\ &\equiv \mathcal{G}\{c(\mathbf{r}', t)\}(\mathbf{r}) \end{aligned} \quad (\text{A1})$$

in 2D for a circular particle. This is a nonlocal equation since the evolution of the field c at the considered point \mathbf{r} in the bulk depends on concentration elsewhere: the knowledge of the field along the bead surface at $r = 1$ and at infinitesimally close points. The latter information is needed to calculate the derivatives of the concentration field. Here

c_k refers to k -th Fourier component, ϕ is the polar angle, and M is a real constant relating the tangential velocity of the fluid and the gradient of c along the bead [16, 17, 19, 21]. The particle velocity is calculated as $(-M\Re c_1(1, t), M\Im c_1(1, t))$. This defines the full evolution of the concentration in the laboratory frame.

Appendix B: Absence of swimming for a variational problem

Here we show the absence of swimming for a variational problem. Suppose we have

$$\dot{c}(x) = \mathcal{G}\{c(x')\}(x), \tag{B2}$$

where

$$\mathcal{G}\{c(x')\}(x) = -\frac{\delta F\{c(x')\}}{\delta c(x)} \tag{B3}$$

for some non-linear functional F , and where $\delta F/\delta c$ refers to functional derivative. Equation (B3) can be rewritten, in view of the very definition of functional derivative, as

$$\begin{aligned} \lim_{h \rightarrow 0} \frac{F\{c(x) + h\delta c(x)\} - F\{c(x)\}}{h} \\ = - \int \mathcal{G}\{c(x')\}(x)\delta c(x)dx. \end{aligned} \tag{B4}$$

B.1 Proof 1

We can write that

$$F\{c(x)\} = F\{c(x+h)\} = F\{c(x) + h\partial_x c(x)\} + O(h^2) \tag{B5}$$

because of the translational invariance of F . Setting δc to $\partial_x c$ in Eq. (B4) and comparing with Eq. (B5) shows that

$$\int \mathcal{G}\{c(x')\}(x)\partial_x c(x)dx = 0. \tag{B6}$$

Multiplying Eq. (B2) by $\partial_x c$ and integrating with respect to x yields

$$\int \dot{c}(x)\partial_x c(x)dx = \int \mathcal{G}\{c(x')\}(x)\partial_x c(x)dx = 0. \tag{B7}$$

Substituting the self-congruent solution $\dot{c}(x) = v\partial_x c(x)$ in Eq. (B7) shows that $v = 0$ unless $\partial_x c(x)$ is zero everywhere.

B.2 Proof 2

The function $F\{c(x, t)\}$ is constant in time for a self-congruent solution due to the invariance of F under rotations and translations of the concentration field c . This expands to

$$\begin{aligned} 0 &= \frac{dF\{c(x, t)\}}{dt} \\ &\equiv \lim_{h \rightarrow 0} \frac{F\{c(x, t+h)\} - F\{c(x, t)\}}{h} \\ &= \lim_{h \rightarrow 0} \frac{F\{c(x, t) + h\dot{c}(x, t)\} - F\{c(x, t)\}}{h} \\ &= - \int \mathcal{G}\{c(x')\}(x)\dot{c}(x)dx = - \int \dot{c}(x)^2 dx, \end{aligned} \tag{B8}$$

where the last equality uses (B2). The right hand side of Eq. (B8) can be equal to zero only if $\dot{c}(x, t) = 0$ for all x . This shows that there are no motile self-congruent solutions of Eq. (B2) with variational right hand side.

Appendix C: Extended analysis of the motility of a segment particle in 1D

We analyze the non-linear dynamics of the 1D model by taking higher-order terms in the expansion (22):

$$\begin{aligned} \mathcal{G}\{c_0(x') + \varepsilon\delta c(x')\}(x) &= \varepsilon\mathcal{G}_1\{\delta c(x')\}(x) \\ &+ \varepsilon^2\mathcal{G}_2\{\delta c(x'), \delta c(x'')\}(x) \\ &+ \varepsilon^3\mathcal{G}_3\{\delta c(x'), \delta c(x''), \delta c(x''')\}(x) + O(\varepsilon^4). \end{aligned} \tag{C9}$$

Here \mathcal{G}_2 and \mathcal{G}_3 are bilinear and trilinear operators, respectively. That is, \mathcal{G}_2 and \mathcal{G}_3 are operators that take, respectively, 2 and 3 functions (here listed inside the curly brackets) of x and return another function of x . They are linear with respect to each variable inside the curly brackets.

We write the time-dependent solution of Eq. (5) as

$$\begin{aligned} c(x, t) &= c_0(x - x_c(t)) + \varepsilon\delta c(x - x_c(t), t), \\ \varepsilon\delta c(x - x_c(t), t) &= \varepsilon\delta c_1(t)f_1(x - x_c(t)) \\ &+ \varepsilon^2 \sum_{i=2}^{\infty} \delta c_i(t)f_i(x - x_c(t)), \end{aligned} \tag{C10}$$

where ε is a small parameter of the expansions and $\delta c_i(t)$ are the amplitudes of the different modes in perturbation. The assumption that the amplitudes of $f_i(x - x_c(t))$ are of order $O(\varepsilon^2)$ for $i > 1$ is validated below by the consistency of equations. The velocity of the comoving frame $\dot{x}_c(t)$ is also small for Pe close to Pe_1 . We further take $Pe - Pe_1 = O(\varepsilon^2)$ for consistency of Eq. (28).

We express the amplitudes $\delta c_i(t)$ for $i > 2$ as a function of $\delta c_1(t)$ by substituting (C9) into the right hand side of Eq. (5) and expanding the result in the basis $f_i(x - x_c(t))$.

$$\begin{aligned} \varepsilon^2\dot{\delta c}_i + O(\varepsilon^3) &= \varepsilon G_1^{(i)}\{\delta c(x')\} + \varepsilon^2 G_2^{(i)}\{\delta c(x'), \delta c(x'')\} \\ &+ O(\varepsilon^3) \\ &= \varepsilon^2 \lambda_i \delta c_i(t) + \varepsilon^2 G_2^{(i)}\{f_1(x'), f_1(x'')\} \delta c_1^2 \\ &+ O(\varepsilon^3), \end{aligned} \tag{C11}$$

where the k -linear functionals $G_k^{(i)}$ are defined by

$$G_k\{\delta c(x'), \dots\}(x) = \sum_{i=0}^{\infty} G_k^{(i)}\{\delta c(x'), \dots\}f_i(x). \tag{C12}$$

The leading term of the right hand side of Eq. (C11) is $\lambda_i \delta c_i(t)$. Since λ_i is negative and has a large absolute value, the solution of (C11) relaxes to a steady-state solution δc_i^0 on a time scale that is small compared to the dynamics of the δc_1 mode. This is where the discrete nature of the set of eigenvalues becomes important: For a finite set, it is always possible to find the eigenvalue with the smallest absolute value and set Pe sufficiently close to Pe_1 to ensure that $|\lambda_1| < |\lambda_i|$ for all i . Since the set of λ_i is infinite, it is not

possible to exclude *a priori* a situation where for any value of $\lambda_1 > 0$ there is another i such that $|\lambda_i| < \lambda_1$. The adiabatic elimination may not work in this case.

We find from Eq. (C11) the steady-state value of δc_i as

$$\delta c_i^0 = -\delta c_1^2 \frac{G_2^{(i)}\{f_1(x'), f_1(x'')\}}{\lambda_i} + O(\varepsilon), \quad (\text{C13})$$

which confirms that the amplitudes of $f_i(x - x_c(t))$ in ansatz (C10) are of order $O(\varepsilon^2)$ for $i > 1$. Note also that $G_2\{f_1(x'), f_1(x'')\}(x)$ is an even function of x , so that $G_2^{(i)}\{f_1(x'), f_1(x'')\} = 0$ if $f_i(x)$ is an odd function. This means that $\delta c_i^0 = O(\varepsilon^3)$ for such values of i .

Equation (C13) is obtained for a fixed value of $\delta c_1(t)$ but it remains approximately valid if $\delta c_1(t)$ is a slowly varying function of time. In particular, it is valid if $\delta c_1(t)$ saturates to a constant.

With $\delta c_i(t)$ for $i > 1$ expressed as functions of $\delta c_1(t)$, the evolution equation (5) for the concentration field (C10) reduces to a closed equation for $\delta c_1(t)$ and $x_c(t)$. The linear analysis of this equation is shown in Sect. 4. The quadratic terms are absent for symmetry reasons. Indeed, substituting (C10) in (5) yields two potential contributions of order $O(\varepsilon^2)$: First, the advection of the solution produces the term $\dot{x}_c(t)\varepsilon\delta c_1(t)\partial_x f_1(x - x_c(t))$ in the left hand side of Eq. (5). This term, as a derivative of an anti-symmetric function, is a symmetric function and thus does not have a $f_1(x - x_c(t))$ component. The second potential contribution comes from the right hand side of Eq. (5), where the term $\varepsilon^2 G_2\{f_1(x'), f_1(x'')\}(x - x_c(t))\delta c_1(t)^2$ is also symmetric. Consequently, the terms of order $O(\varepsilon^3)$ are the next order after the linear terms. There are so many different terms at this order that listing them in general case would not be practical but it is easy to show that each of them can be reduced to terms proportional to $\varepsilon^3\delta c_1(t)^3$. This yields the Eq. (28).

References

1. M.C. Marchetti, J.-F. Joanny, S. Ramaswamy, T.B. Liverpool, J. Prost, M. Rao, R.A. Simha, Hydrodynamics of soft active matter. *Rev. Mod. Phys.* **85**(3), 1143 (2013)
2. E. Lauga, T.R. Powers, The hydrodynamics of swimming microorganisms. *Rep. Prog. Phys.* **72**, 096601 (2009)
3. E. Lauga, W.R. DiLuzio, G.M. Whitesides, H.A. Stone, Swimming in circles: Motion of bacteria near solid boundaries. *Biophys. J.* **105**, 069401 (2006)
4. N.P. Barry, M.S. Bretscher, Dictyostelium amoebae and neutrophils can swim. *Proc. Natl. Acad. Sci.* **107**(25), 11376–11380 (2010)
5. P.R. O'Neill, J.A. Castillo-Badillo, X. Meshik, V. Kalyanaraman, K. Melgarejo, N. Gautam, Membrane flow drives an adhesion-independent amoeboid cell migration mode. *Dev. Cell* **46**(1), 9–224 (2018). <https://doi.org/10.1016/j.devcel.2018.05.029>
6. L. Aoun, P. Negre, A. Farutin, N. Garcia-Seyda, M.S. Rivzi, R. Galland, A. Michelot, X. Luo, M. Biarnes-Pelicot, C. Hivroz, S. Rafai, J.-B. Sibaret, M.-P. Valignat, C. Misbah, O. Theodoly, Mammalian amoeboid swimming is propelled by molecular and not protrusion-based padding in lymphocytes. *Biophys. J.* **119**, 1157–1177 (2020). <https://doi.org/10.1101/509182>
7. H.S. Jennings, On the significance of spiral swimming of organisms. *Am. Soc. Natl.* **35**, 369 (1901)
8. V.B. Shenoy, D.T. Tambe, A. Prasad, J.A. Theriot, A kinematic description of the trajectories of listeria monocytogenes propelled by actin comet tails. *Proc. Natl. Acad. Sci.* **104**(20), 8229–8234 (2007). <https://doi.org/10.1073/pnas.0702454104>
9. I.H. Riedel, K. Kruse, J. Howard, A self-organized vortex array of hydrodynamically entrained sperm cells. *Science* **309**(5732), 300–303 (2005). <https://doi.org/10.1126/science.1110329>
10. S. Jana, S.H. Um, S. Jung, Paramecium swimming in capillary tube. *Phys. Fluids* **24**(4), 041901 (2012)
11. C. Krüger, G. Klös, C. Bahr, C.C. Maass, Curling liquid crystal microswimmers: a cascade of spontaneous symmetry breaking. *Phys. Rev. Lett.* **117**(4), 048003 (2016)
12. H. Löwen, Chirality in microswimmer motion: from circle swimmers to active turbulence. *Eur. Phys. J. Spec. Top.* **225**(11), 2319–2331 (2016). <https://doi.org/10.1140/epjst/e2016-60054-6>
13. M. Suga, S. Suda, M. Ichikawa, Y. Kimura, Self-propelled motion switching in nematic liquid crystal droplets in aqueous surfactant solutions. *Phys. Rev. E* **97**(6), 062703 (2018)
14. N. Narinder, C. Bechinger, J.R. Gomez-Solano, Memory-induced transition from a persistent random walk to circular motion for achiral microswimmers. *Phys. Rev. Lett.* **121**(7), 078003 (2018)
15. Z. Izri, M.N. Van Der Linden, S. Michelin, O. Dautot, Self-propulsion of pure water droplets by spontaneous Marangoni-stress-driven motion. *Phys. Rev. Lett.* **113**(24), 248302 (2014)
16. W.F. Hu, T.S. Lin, S. Rafai, C. Misbah, Chaotic swimming of phoretic particles. *Phys. Rev. Lett.* **123**, 238004 (2019)
17. S. Michelin, E. Lauga, D. Bartolo, Spontaneous autophoretic motion of isotropic particles. *Phys. Fluids* **25**, 061701 (2013)
18. S. Michelin, E. Lauga, Phoretic self-propulsion at finite Peclet numbers. *J. Fluid Mech.* **747**, 572–604 (2014). <https://doi.org/10.1017/jfm.2014.158>
19. M. Schmitt, H. Stark, Swimming active droplet: a theoretical analysis. *EPL (Europhysics Letters)* **101**(4), 44008 (2013)
20. C. Jin, C. Krüger, C.C. Maass, Chemotaxis and autochemotaxis of self-propelling droplet swimmers. *Proc. Natl. Acad. Sci.* **114**(20), 5089–5094 (2017). <https://doi.org/10.1073/pnas.1619783114>
21. M. Morozov, S. Michelin, Nonlinear dynamics of a chemically-active drop: from steady to chaotic self-propulsion. *J. Chem. Phys.* **150**(4), 044110 (2019)
22. M. Morozov, S. Michelin, Self-propulsion near the onset of Marangoni instability of deformable active droplets. *J. Fluid Mech.* **860**, 711–738 (2019). <https://doi.org/10.1017/jfm.2018.853>
23. M. Morozov, Adsorption inhibition by swollen micelles may cause multistability in active droplets. *Soft Matter* **16**, 5624–5632 (2020)
24. Y. Chen, K.L. Chong, L. Liu, R. Verzicco, D. Lohse, Instabilities driven by diffusiophoretic flow on catalytic surfaces. *J. Fluid Mech.* **919**, 10 (2021). <https://doi.org/10.1017/jfm.2021.370>
25. B.V. Hokmabad, R. Dey, M. Jalaal, D. Mohanty, M. Almkambetova, K.A. Baldwin, D. Lohse, C.C. Maass,

- Emergence of bimodal motility in active droplets. *Phys. Rev. X* **11**, 011043 (2021). <https://doi.org/10.1103/PhysRevX.11.011043>
26. A. Izzet, P.G. Moerman, P. Gross, J. Groenewold, A.D. Hollingsworth, J. Bibette, J. Brujic, Tunable persistent random walk in swimming droplets. *Phys. Rev. X* **10**, 021035 (2020). <https://doi.org/10.1103/PhysRevX.10.021035>
 27. A.Y. Rednikov, Y.S. Ryazantsev, M.G. Velarde, Drop motion with surfactant transfer in a homogeneous surrounding. *Phys. Fluids* **6**(2), 451–468 (1994)
 28. A. Golovin, Y.P. Gupalo, Y.S. Ryazantsev, Change in shape of drop moving due to the chemithermocapillary effect. *J. Appl. Mech. Tech. Phys.* **30**(4), 602–609 (1989)
 29. P. Maiuri, J.-F. Rupprecht, S. Wieser, V. Ruprecht, O. Bénichou, N. Carpi, M. Coppey, S. De Beco, N. Gov, C.-P. Heisenberg, C. Lage Crespo, F. Lautenschlaeger, M. Le Berre, A.-M. Lennon-Dumenil, M. Raab, H.-R. Thiam, M. Piel, M. Sixt, R. Voituriez, Actin flows mediate a universal coupling between cell speed and cell persistence. *Cell* **161**(2), 374–386 (2015). <https://doi.org/10.1016/j.cell.2015.01.056>
 30. P. Recho, T. Putelat, L. Truskinovsky, Contraction-driven cell motility. *Phys. Rev. Lett.* **111**(10), 108102 (2013)
 31. P. Recho, L. Truskinovsky, Maximum velocity of self-propulsion for an active segment. *Math. Mech. Solids* (2015). <https://doi.org/10.1177/1081286515588675>
 32. R.J. Hawkins, R. Poincloux, O. Bénichou, M. Piel, P. Chavrier, R. Voituriez, Spontaneous contractility-mediated cortical flow generates cell migration in three-dimensional environments. *Biophys. J.* **101**(5), 1041–1045 (2011)
 33. A.C. Callan-Jones, V. Ruprecht, S. Wieser, C.P. Heisenberg, R. Voituriez, Cortical flow-driven shapes of non-adherent cells. *Phys. Rev. Lett.* **116**, 028102 (2016). <https://doi.org/10.1103/PhysRevLett.116.028102>
 34. A. Farutin, J. Etienne, C. Misbah, P. Récho, Crawling in a fluid. *Phys. Rev. Lett.* **123**, 118101 (2019)
 35. G. Negro, A. Lamura, G. Gonnella, D. Marenduzzo, Hydrodynamics of contraction-based motility in a compressible active fluid. *EPL* **127**(5), 58001 (2019). <https://doi.org/10.1209/0295-5075/127/58001>
 36. G.B. Blanchard, J. Étienne, N. Gorfinkiel, From pulsatile apicomedial contractility to effective epithelial mechanics. *Curr. Opin. Genet. Dev.* **51**, 78–87 (2018). <https://doi.org/10.1016/j.gde.2018.07.004>
 37. A.M. Menzel, H. Löwen, Traveling and resting crystals in active systems. *Phys. Rev. Lett.* **110**, 055702 (2013). <https://doi.org/10.1103/PhysRevLett.110.055702>
 38. A.M. Menzel, T. Ohta, H. Löwen, Active crystals and their stability. *Phys. Rev. E* **89**, 022301 (2014). <https://doi.org/10.1103/PhysRevE.89.022301>
 39. L. Ophaus, S.V. Gurevich, U. Thiele, Resting and traveling localized states in an active phase-field-crystal model. *Phys. Rev. E* **98**, 022608 (2018). <https://doi.org/10.1103/PhysRevE.98.022608>
 40. C. Misbah, M.S. Rizvi, W.F. Hu, T.S. Lin, S. Rafai, A. Farutin, Universal Trajectories of Motile Particles Driven by Chemical Activity. *arXiv preprint arXiv:2112.13801* (2021)
 41. A. Farutin, M.S. Rizvi, W.-F. Hu, T.S. Lin, S. Rafai, C. Misbah, A reduced model for a phoretic swimmer. *J. Fluid Mech.* **952**, 6 (2022). <https://doi.org/10.1017/jfm.2022.870>
 42. S. Saha, E. Yariv, O. Schnitzer, Isotropically active colloids under uniform force fields: from forced to spontaneous motion. *J. Fluid Mech.* **916**, 47 (2021). <https://doi.org/10.1017/jfm.2021.222>
 43. A. Farutin, C. Misbah, Singular bifurcations: a regularization theory. *arXiv:2112.12094* (2021)

Springer Nature or its licensor (e.g. a society or other partner) holds exclusive rights to this article under a publishing agreement with the author(s) or other rightsholder(s); author self-archiving of the accepted manuscript version of this article is solely governed by the terms of such publishing agreement and applicable law.